

Ultrathin gold nanowires for transparent electronics

Dissertation
zur Erlangung des Grades
des Doktors der Ingenieurwissenschaften
der Naturwissenschaftlich-Technischen Fakultät
der Universität des Saarlandes

von
Johannes H. M. Maurer

Angefertigt am
INM – Leibniz–Institut für Neue Materialien

Saarbrücken
2017

Tag des Kolloquiums: 19.09.2017

Dekan: Prof. Dr. G. Kickelbick

1. Berichterstatter: Prof. Dr. T. Kraus

2. Berichterstatter: Prof. Dr. E. Arzt

Vorsitz: Prof. Dr. W. Possart

Akad. Mitarbeiter: Dr.-Ing. M. Zamanzade

**„Der Sinn und das Kennzeichen echter
Wissenschaft besteht nach meiner Meinung
in den nützlichen Erfindungen, die man
daraus herleiten kann.“**

Gottfried Wilhelm Leibniz

Publications and contribution report

This thesis has been published partially in four publications, which are referred to in the text by their letter. The author declares his contributions to the publications included in this thesis in the following.

(A) Sintering of Ultrathin Gold Nanowires for Transparent Electronics.

Maurer, J. H. M.; González-García, L.; Reiser, B.; Kanelidis, I.; Kraus, T.

ACS Appl. Mater. Interfaces 2015, 7, 7838–7842.

Contribution of Johannes H. M. Maurer: He designed the study and performed all experiments. He conceived and wrote the manuscript.

(B) Ultrathin Gold Nanowires for Transparent Electronics: Soft Sintering and Temperature Stability.

Maurer, J. H. M.; González-García, L.; Reiser, B.; Kanelidis, I.; Kraus, T.

Phys. Status Solidi (a) **2016**, 213, 2336–2340.

Contribution of Johannes H. M. Maurer: He designed the study and performed all experiments. He conceived and wrote the manuscript.

(C) Templated Self-Assembly of Ultrathin Gold Nanowires by Nanoimprinting for Transparent Flexible Electronics.

Maurer, J. H. M.; González-García, L.; Reiser, B.; Kanelidis, I.; Kraus, T.

Nano Lett. **2016**, 16, 2921–2925.

Contribution of Johannes H. M. Maurer: He designed the study and performed all experiments. He conceived and wrote the manuscript.

(D) Direct nanoimprinting of a self-organizing nanowire ink for transparent, flexible electronics.

Maurer, J. H. M.; González-García, L.; Backes, I. K.; Reiser, B.; Schlossberg, S. M.; Kraus, T.

Adv. Mater. Technol. **2017**, 1700034

Contribution of Johannes H. M. Maurer: He designed the study and performed the printing experiments on PET and cling wrap. He designed the printing setup, built the touch sensors, and characterized all the layers. He conceived and wrote the manuscript.

Abstract

Transparent electrodes (TEs) are key components of modern optoelectronic devices like touch screens, solar cells, and OLEDs, but an inherent trade-off between high electrical conductivity and optical transparency limits the available material range. Indium tin oxide (ITO) has been dominating the market, but cannot provide the mechanical flexibility that novel devices based on polymer substrates require; high process temperatures required for high-grade ITO exceed the thermal budget of many polymers. Solution-processed metal grids from nanoscale building blocks are a promising alternative providing superior mechanical flexibility at cost-effective and scalable fabrication with low thermal budget.

For this dissertation, ultrathin gold nanowires (AuNWs) from wet-chemical synthesis were explored as novel base material for TEs. Plasma sintering was shown to ameliorate the wires' high contact resistances and poor stability. A novel nanoimprinting process was developed to pattern AuNWs into grids. The method relies on the large flexibility of the AuNWs and their ability to self-assemble into continuous hierarchical superstructures in the cavities of a pre-patterned elastomeric stamp. The process yielded ordered grids with submicron linewidth at low thermal budget, thus going beyond state-of-the-art printed grids. The grids also showed competitive optoelectronic properties and superior mechanical flexibility to the incumbent materials and were applied as TEs in touch sensors.

Zusammenfassung

Transparente Elektroden (TE) sind Schlüsselbauteile moderner optoelektronischer Geräte wie Touchscreens, Solarzellen oder OLEDs. Es besteht jedoch ein intrinsischer Zielkonflikt zwischen elektrischer Leitfähigkeit und optischer Transparenz, was die Auswahl an verfügbaren Materialien stark eingrenzt. Indium-Zinn-Oxid (ITO), welches bis heute den Markt dominiert, kann die mechanische Flexibilität neuer Geräte basierend auf Polymersubstraten nicht gewährleisten; die für hochwertiges ITO benötigten Prozesstemperaturen übersteigen oft die thermische Beständigkeit vieler Polymere. Nassbeschichtete Metallgitter aus nanoskaligen Bausteinen sind eine vielversprechende Alternative: sie weisen höhere mechanische Flexibilität auf und können durch kosteneffiziente und skalierbare Prozesse bei niedrigen Temperaturen hergestellt werden.

In der vorliegenden Dissertation wurden ultradünne Gold Nanodrähte (AuNWs) aus nasschemischer Synthese als neuartige Bausteine für TE untersucht. Durch Plasmasintern konnten die hohen Kontaktwiderstände und geringe Stabilität der AuNWs verbessert werden. Ein neuartiger Nanopräge-Prozess wurde entwickelt, um AuNWs zu Gittern zu strukturieren. Die Methode beruht auf der hohen Flexibilität der AuNWs und deren Fähigkeit sich zu kontinuierlichen, hierarchischen Überstrukturen in den Zwischenräumen eines vorstrukturierten Stempels selbst anzuordnen. Mit dem Prozess wurden geordnete Gitter mit Linienbreiten unter einem Mikrometer unter geringer thermischer Einwirkung hergestellt. Die Gitter haben konkurrenzfähige optoelektronische Eigenschaften zu den vorherrschenden Materialien bei überlegener mechanischer Flexibilität und wurden als TE in berührungsempfindlichen Sensoren verbaut.

Acknowledgements

First of all, I am very grateful to my “Doktorvater” *Prof. Tobias Kraus*, genius scientist, polymath, and gourmet, who always kept the right balance between colleague and boss creating a pleasant and productive working atmosphere during the entire time. Thank you very much for giving me the opportunity to write my dissertation in the “structure formation group” and your valuable guidance and advices during the last three years. Thank you for the generous support of international conferences and workshops, which should not be taken for granted.

I am grateful to *Prof. Eduard Arzt* for giving me the opportunity to write my dissertation at the INM and the willingness to act as second reviewer. Prof. Arzt was a constant companion of my career as material scientist starting with his lecture slides that laid the fundamentals of materials science during my Bachelor studies in Stuttgart, as official supervisor of my master thesis, and now as reviewer of my dissertation. Thank you very much for your support.

Many thanks go to my “scientific advisor” *PD Dr.-Ing. Guido Falk*, head of the research group of structural and functional ceramic at Saarland University, for the various pleasant scientific discussions during my PhD.

Special thanks go to the “Nanospekt” project team, better known as “Nanospekt family”, which expresses to me much better the close relation and friendship we have developed during the last 3 years. I think we were a great team of scientists, office mates, and friends: First of all, the “mother”, *Dr. Lola González-García*, supervisor, mentor, and friend with the genius nose for the right (publication) story. Without her, I would not have been able to write the thesis the way it is now. Thank you very much for guiding me during my thesis, your help with the Rhino 3D figures, and the energized discussions about science and many other topics...;-). Thanks also for teaching me the most important expressions in Spanish ;-). The “father” *Dr. Ioannis Kanelidis*, “Kanela”, “lab president” and best “Kritharaki” cook. Thanks for your help with the wire synthesis, the Raman measurements and the epic “Kanelidis mix” that facilitated every lab cleaning. The “sister” *Beate (Haas) Reiser*, co-PhD student in the project, who shared with me the good and bad days of a life as PhD student. Her work on the synthesis laid the foundations of the work on AuNWs. Thank you for your help and chemistry advices.

Sebastian Beck, “BeckNorris”, the engineer in our team, multi-talented problem-solver and huge Globus-Fleischkäsweck-Fan ;). Thanks for your help with the nanoimprinting setup and the CAPA tool.

Many thanks go to the master students and student assistants of “Team Nanospekt” who directly contributed to the work for this thesis: *Indra Backes*, who helped with incredible enthusiasm in the scale-up of the imprinting process during her master thesis; *Sarah Schlossberg*, exchange student from UCSD, who advanced the printing on flexible substrates; *Manuel Hawner* for his help with the molding of the PDMS stamp.

Many thanks go to the rest of the structure formation group. I think we had an amazing working atmosphere and we were a great mixture of outstanding characters: *Gabi Koster*, secretary and “mother” of the group, efficient, competent and unbelievably nice. Thanks for perfect organization of the group and your constantly positive charisma. Many thanks go to my colleagues as PhD students: *Dr. Dominik Gerstner*, “Dojo G”, already graduated, SAXS expert and great fan of steak haché and artificial banana flavor. Thanks for your help with analyzing SAXS data and for great time at the synchrotron (still jealous of Nina’s lunch bag). *Aljosha Rakim-Jochem*, “de Chef”, awesome chemist and passionate delegator ;-). Thanks for many valuable discussions about science and life, but also for great “nonsense talk” in the lab that made hard days in the lab more enjoyable. *Thomas Kister*, “Supraman”, the perfect fusion of Bud Spencer and MacGyver, genius doer that can synthesize particles with vanishingly small polydispersity and any ligand you want. He is the guy you should call if you have any problems...he will fix it with Epoxy glue. *Andreas Hegetschweiler*, the “Swiss Saarlandian”, constantly trying to kid each other, which made the work days always more fun. Thanks for taking over the exam corrections. *Juraj Drzic*, “J”, the new PhD student in the Nanospekt project and office mate. *Robert Strahl*, “engineer 2.0” in the Nanospekt team, thanks for your help with various engineering tasks. Many thanks go to our lab technicians: *Anika Kleemann*, “lab dragon” or “lab mum”, but definitely “lab head” and group organizer. I don’t want to imagine how the labs would have looked like without your constant care. Thank you very much for your help synthesizing gold acid and particles. The same holds for *Nicole Schiff* and *Kathrin Alt*. Thank you very much for your help in the lab, the ordering of chemicals and your constant smile ☺. Many thanks go also to: *Dr. Daniel Brodoceanu*, the “laser guy”; thank you for many inspiring conversations in the lab (if you talk 10 min with him, you will have more ideas than you can ever im-

plement). *Dr. Genesis Ankah*, “The FIBber”; thanks for your help sputtering electrodes in the FIB. *Dr. David Doblas-Jiménez*, *Dr. Peng Zhang*, *Dr. Thibaut Thai*, *Dr. Manuel Oliva*, *Dr. Alberto Escudero*, *Dr. Vikrant Naik*, *Anna Zimmermann*, *Jonas Hubertus*, *Jona Engel*, *Anna Heib*, *Christopher Scherrer*, *Andrea Pyttlik*, *Lars-Arne Meyer*, *Lukas Engel* and *Thilo Grammes* for the nice times together in the lab.

Many thanks go to: *Diana Löb* and *Silvia de Graaf*, the secretaries of Prof. Arzt, for the perfect PhD administration; *Dr. Sabine Heusing*, the “queen” of the UV-Vis, for her help with the optical characterization; *Dr. Thiago Martins Amaral* for his help with the setup for the capacitive touch screen; *Jenny Kampka* for providing the PET foil; *Sarah Fischer* for helping with the PDMS stamps; *Dr. Marcus Koch* for his help with SEM analysis; *Dr. Johanna Blass*, *Dr. Arzu Colak*, and *Marius Gipperich* for their help with the AFM analysis; *Simon Fleischmann* for his help with the Raman measurements; *Miriam Badziong* for great bookings of the business trips.

I am very grateful to *Dr. Heiko Wolf* and *Songbo Ni* from IBM Research – Zurich for the warm welcome and great weeks of creative research and fun during my visit at the IBM laboratories. Many thanks go to the DAAD and the “GradUS global” program of the Saarland University for the funding of the visit.

Many thanks go to my *friends* that were constantly “available” to overcome a frustrating lab day with “a beer from my hometown” and the awesome “Spaghetti Nauwies” in the eponymous bistro. I am certainly going to miss the WhatsApp-message: “11:30 Mensa?”

I am particularly grateful to my *parents*. Thank you for unlimited support during the last 29 years!!! I am grateful also to my *sister Christine* who has always shared the thrill with me, if a paper was going to be accepted or not. Thanks for the epic “evil eatings” after each publication ;-).

There are no proper words to describe the deepest gratitude I owe to my wife *Isabelle* who continuously managed to make me laugh and feel happy even at days when everything failed in the lab. THANK YOU!

Table of contents

1	INTRODUCTION AND MOTIVATION.....	1
2	THEORY AND STATE OF THE ART.....	5
2.1	Transparent electrodes.....	5
2.1.1	Modern applications and requirements	5
2.1.2	Transparency-conductivity trade-off.....	10
2.1.3	Transparent conductive oxides.....	11
2.1.4	Solution-based transparent electrodes for flexible devices.....	12
2.1.4.1	Random metal nanowire networks.....	14
2.1.4.2	Ordered metal grids.....	16
2.2	Patterning of nanoparticle inks for electronics.....	19
2.2.1	Fabrication of transparent metal grids from nanoparticle inks	19
2.2.2	Direct nanoimprinting of nanoparticles	22
2.3	Sintering of nanoparticle inks for electronics	26
2.3.1	Photonic sintering	27
2.3.2	Chemical sintering	29
2.3.3	Plasma sintering	30
2.4	Ultrathin gold nanowires (AuNWs).....	32
2.4.1	Synthesis and growth mechanism	32
2.4.2	Self-assembly	36
2.4.3	AuNWs for transparent electronics.....	36
3	RESULTS.....	39
3.1	Publication A: Sintering of Ultrathin Gold Nanowires for Transparent Electronics.....	39

3.2	Publication B: Ultrathin Gold Nanowires for Transparent Electronics: Soft Sintering and Temperature Stability.	41
3.3	Publication C: Templated Self-Assembly of Ultrathin Gold Nanowires by Nanoimprinting for Transparent Flexible Electronics.	43
3.4	Publication D: Direct Nanoimprinting of a Colloidal Self-organizing Nanowire Ink for Transparent, Flexible Electronics.	45
4	DISCUSSION	47
4.1	Sintering of AuNWs	47
4.2	Patterning of AuNWs	50
5	CONCLUSIONS	53
6	OUTLOOK	55
7	BIBLIOGRAPHY	57
8	APPENDIX	69
8.1	List of abbreviations and symbols	69
8.2	Sheet resistance.....	71
8.3	List of publications	72
8.4	Conference contributions.....	73

1 Introduction and motivation

Since the first iPhone was introduced in 2007 by Apple, smartphones have become an integral part of our daily life. A recent study in the United Kingdom revealed that we spend on average 3 hours and 16 minutes per day with our smartphone.¹ An essential component for the human-machine interaction is the touch-sensitive display, which acts as user interface in many other devices, too, including tablets, e-book readers, or car entertainment systems. Integral parts of the touch screens are “transparent electrodes”: materials that conduct electricity, but are at the same time transparent to visible light.² Such materials are also prerequisites for the functionality of numerous other optoelectronic devices such as organic light-emitting diodes and solar cells (section 2.1.1).

The range of available materials that combine high optical transparency and good electrical conductivity is limited because both properties are connected: materials with good electrical conductivity like metals, for instance, are usually opaque in bulk state because high carrier concentrations imply strong optical absorption (section 2.1.2). Doped metal oxides represent a unique class of materials that combine transparency and conductivity. In particular, tin-doped indium oxide (ITO) evolved into the predominantly used material for transparent electrodes today (section 2.1.3).³

The trend towards flexible and organic devices based on polymer substrates sets new challenges: foldable displays, wearable touch screens, and bendable solar cells require transparent electrodes to be mechanically flexible, and their fabrication must not exceed the thermal budget of polymer substrate. ITO and other transparent oxides do not meet these requirements due to their ceramic brittleness and the often high process temperatures. Many alternatives to ITO have been proposed including conductive polymers, carbon materials, and metal grids, among others (section 2.1.4). Bottom-up fabrication, where conductive nanostructures (e.g. metal nanoparticles) get deposited from liquid dispersions (“inks”) have been reported as a promising approach: solution-processing allows for cost-effective and scalable fabrication at low thermal budget; additive deposition of particles reduces the required amount of material.⁴ In particular, random metal

nanowire networks (section 2.1.4.1) and ordered metal grids (section 2.1.4.2) made from nanoscale building blocks are potential competitors for ITO, combining high electrical conductivity, optical transparency, and mechanical flexibility.⁵

Bottom-up fabrication of electronic features from metal nanoparticle inks usually involves two steps:

(1) Controlled deposition of the particles: Precise patterning is important for device performance, but deterministic assembly of individual particles is challenging due to their nanometer-size. Novel methods have been developed to precisely deposit conductive patterns from nanoparticle inks following the concepts of traditional printing (“printed electronics”) (section 2.2).

(2) Sintering to reduce contact resistances: After synthesis, nanoparticles are generally capped by organic molecules, which lend them the necessary colloidal stability in dispersion, but at the same time provoke high contact resistances between individual nanoparticles. Hence, nanoparticle layers usually have to be annealed after deposition to remove the ligands or modify them (section 2.3).

Today’s inks prevalently consist of spherical metal nanoparticles that provide high particle mobility and good printability. Anisotropic particles with high aspect ratios could ease percolation and reduce the number of insulating junctions at particle-particle interfaces. Stiff wires impede printing, however. Commercially available silver nanowires, for instance, are usually randomly dispensed to form networks like “pick-up sticks”, which provides only little control over the network geometry.

Ultrathin gold nanowires (AuNWs) that have recently become available from wet-chemical synthesis are an alternative base material: they combine ultra-high aspect ratios (> 1000) with high particle mobility and mechanical flexibility through their small diameter (< 2 nm) (section 2.4). The initial publications on AuNW thin-films showed their ability to form highly transparent thin films, but insulating oleylamine ligand shell caused high contact resistances between the individual wires; sheet resistances in the $M\Omega$ range were reported. Their small diameter makes them susceptible to fragmentation by the Rayleigh instability, too.

In this thesis, I explore the use of AuNWs as building blocks for the fabrication of transparent electrodes addressing the two steps for bottom-up fabrication:

- (1) Sintering to reduce contact resistances between wires and increase the stability of AuNW thin films (publications A and B).
- (2) Patterning of the wires into high resolution metal grids (publications C and D).

2 Theory and state of the art

2.1 Transparent electrodes^a

Early scientific reports on ultrathin transparent and conductive metal films can be found at the end of the 19th century.⁶ Applications of transparent electrodes (TEs) appeared first with the advent of the electronics industry during World War II. Transparent conductive oxides were used as transparent heaters for the de-icing of cockpit windows.³ In the following centuries, consumer electronics and energy applications stimulated the research on TEs with the emergence of flat-panel display technology and solar cells. Doped oxides, particularly ITO, were shown to uniquely combine transparency and conductivity and became the leading material. In the last decades, TE development has been fueled by the growing market of modern optoelectronic applications like smartphones, smart TVs, thin-film organic solar cells, and large-area organic lighting.² Novel solution-based TEs are challenging the incumbent ITO that struggles with the requirements of future flexible, polymer-based devices.

2.1.1 Modern applications and requirements

In this section, the role of TEs in the four most relevant modern optoelectronic devices will be discussed and the respective requirements deduced. Figure 1 shows schematic diagrams of the basic device architectures of resistive and capacitive touch sensors, organic solar cells (OSCs), and organic light emitting diodes (OLEDs).

The field of **touch sensors** is a rapidly growing market for TEs. The applications range from consumer electronics including mobile phones, notebooks, and tablets to household electronics like coffee makers, microwaves, or home entertainment systems that more and more get equipped with touch-sensitive screens. Market forecasts predict that

^a Many terms have been used to describe materials with concomitant optical transparency and electrical conductivity, including “Transparent Conductive Materials (TCMs)”, “Transparent Electrodes (TEs)”, “Transparent Conducting Films (TCFs)”, “Transparent Conductive Electrodes (TCEs)”, and “Transparent Conducting Coatings (TCCs)”, amongst many others. Each term emphasizes slightly different aspects. In this thesis, the term “Transparent Electrodes (TEs)” will be solely used as it appears to be the most common.

the surface area of worldwide produced touch screens will double between 2014 and 2025, reaching more than 80 km² in 2025.⁷

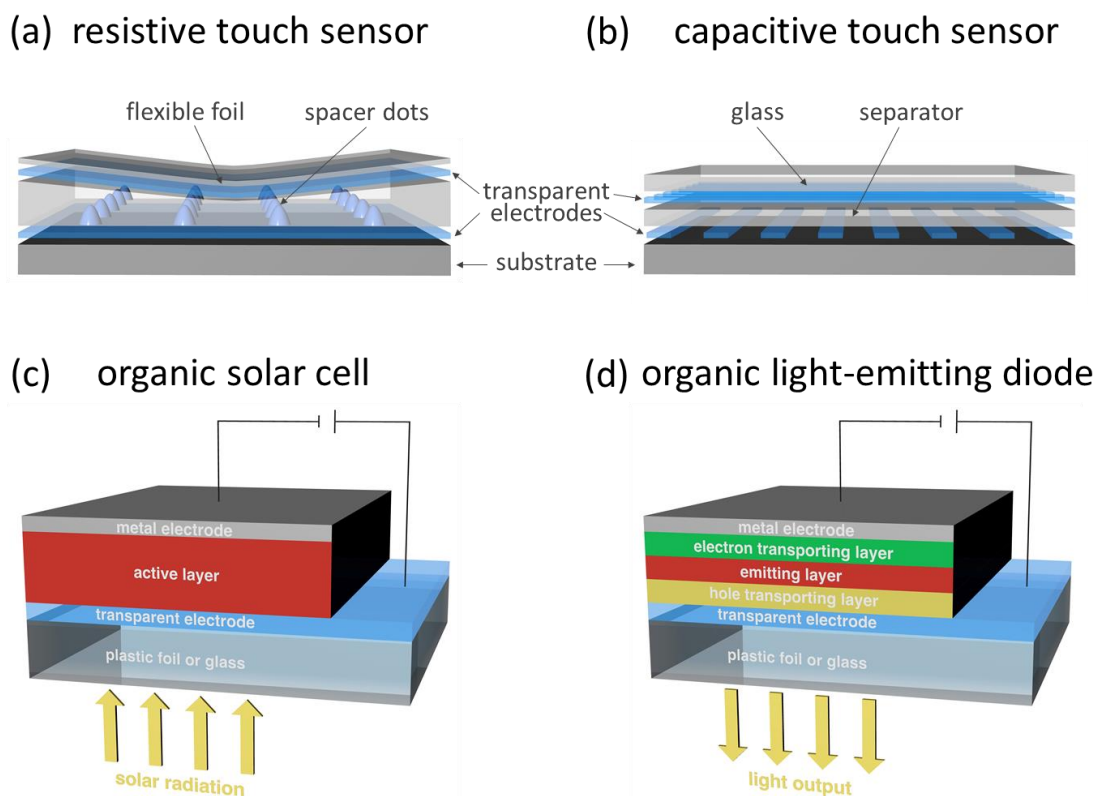


Figure 1: Schematic diagrams of (a) a resistive touch sensor, (b) a capacitive touch sensor, (c) an organic solar cell, and (d) an organic light-emitting diode.^a

Touch screens are generally composed of a visual display and the actual touch sensor layered on top of it. The touch sensors can be subdivided into resistive and capacitive touch sensors with multiple different variations. In the simplest case, a resistive touch sensor consists of two TEs, one of which has to be flexible and is usually deposited onto a polymer foil (see Figure 1a). The two electrodes are separated by “spacer dots” that are usually between 10-100 μm in radius and 1-2.5 mm apart. When pressing the upper electrode down, the two TEs come into contact and act as voltage divider at this position. By measuring the voltage changes at the edges of the electrodes, the x - y position of the touch point can be determined. Capacitive touch sensors (mutual capacitance) usually consist of two separated TEs that are patterned to form an x - y matrix (Figure 1b). When touching the sensor with a finger or a conductive pen, the change in capacitance

^a The schemes present simplified architectures and should only serve as models to understand the fundamental concepts and the role of TEs in the devices.

at each electrode is measured and the exact touch position can be determined. Future trends include large-area and flexible touch screens, as well as high resolution screens.⁸

Though still limited in efficiency and lifetime, **organic solar cells (OSCs)** have gained interest due to their potential to be fabricated on flexible substrates and large-areas by cost-effective roll-to-roll solution-phase processing.⁹ The basic architecture of organic solar cells (Figure 1c) consists of two electrodes that enclose an active layer in which light energy is converted into electricity by the photovoltaic effect. The active layer may be a single layer, bilayer, or a bulk heterojunction, amongst others.¹⁰ The electrode facing the sun light should have minimum photon absorption to increase the efficiency of the cell. The second electrode can be intransparent and is usually made from metals like Al, Mg, or Cu. For solar cells, correct adjustment of the work functions of the different layers is indispensable for an efficient operation.¹¹ Future visions include fully transparent, flexible solar cells that are fabricated by wet methods and can be coated on windows and curved polymer substrates.

Organic light emitting diodes (OLEDs) outperform conventional liquid crystal displays (LCDs) regarding brightness, efficiency, contrast, and, important for novel designs, mechanical flexibility.¹² The general architecture of OLEDs is akin to solar cells: an active layer is sandwiched between two electrodes, one of which has to be transparent (Figure 1d). While in solar cells electron-hole pairs are created in the active layer, OLEDs rely on their recombination to create photon emission. The active layer is often a multilayer system composed of a hole transporting layer, an emitting layer, and an electron transporting layer. Photon emission out of the device requires a transparent electrode.¹³ Future trends comprise all solution-processed large-area lighting (wallpaper displays or curtains), as well as rollable and portable displays.

Requirements for transparent electrodes

Transparent electrodes are primarily evaluated by two major properties: **optical transmittance** T (%)^a and **electrical sheet resistance** R_s (Ω/sq)^b. The requirements for both properties strongly depend on the specific application.¹⁴ A rough classification has been reported by Hu et al.:¹⁵

- The optical transmittance should generally be $\geq 90\%$ in the visible range for all devices. For comparison, values are usually given for a specific wavelength (mostly at 500 or 550 nm). High optical transmittance is needed to ensure bright display images in touch screens, increased power conversion efficiency in solar cells and high external quantum efficiency in OLEDs.
- The required sheet resistances (R_s) vary by several orders of magnitude: For touch screen applications, a sheet resistance in the range of 400–1000 Ω/sq is sufficient for operation. A highly uniform electrical response of the TE must be guaranteed for accurate touch sensing. OLEDs and solar cells require lower sheet resistance ($R_s \leq 10 \Omega/\text{sq}$). High resistance would cause resistive heating and a non-uniform emission in OLEDs; solar cells would suffer from decreased efficiency as their performance relies on effective carrier collection before recombination and low cell series resistance.^{16–18}

Several criteria (figures of merit) have been proposed to compare the performance of TEs from different materials systems and processes regarding transparency and conductivity.¹⁹ Most used today is a metric based on the theory of Glover and Tinkham that describes the transmittance T as a function of the sheet resistance R_s by

$$T = \left(1 + \frac{Z_0}{2R_s} \frac{\sigma_{op}}{\sigma_{dc}} \right)^{-2}$$

^a The total optical transmittance T_{tot} is defined as the ratio $T_{\text{tot}} = I_T/I_0$ of the intensity of light transmitted through a material (I_T) to the intensity of the incident light (I_0) and is usually given in % ($\%T = I_T/I_0 \times 100$). The total transmittance T_{tot} can be subdivided into the ballistic transmittance T_{bal} that accounts for the light transmitted parallel to the incoming beam and the diffuse transmittance T_{dif} that accounts for the diffuse transmitted light ($T_{\text{tot}} = T_{\text{bal}} + T_{\text{dif}}$). For TEs, the ballistic optical transmittance is the most relevant parameter. It is usually simply given as “(optical) transmittance T ” in literature, which has been adopted for this thesis, unless stated explicitly otherwise.

^b The sheet resistance has been introduced as a measure of resistance for thin films with homogeneous thickness and is defined as $R_s = \frac{\rho}{t}$ with the resistivity ρ and the film thickness t . See section 8.2 for further information.

with Z_0 ($= 377 \Omega$) being the vacuum impedance and σ_{dc} and σ_{op} the optical and dc conductivities of the material.^{20–22} The transmittance T is measured in the visible wavelength range and mostly given at $\lambda = 550$ nm. The ratio σ_{dc}/σ_{op} serves as **figure of merit**. The theory of Glover has been extended and refined for specific systems in recent studies.^{19,23}

Other important properties include:

- The “**haze**”, which quantifies the fraction of transmitted light scattered at wide angles and is usually defined as the ratio between diffuse and total transmittance.^a The required haze value strongly depends on the application: Touch screens, for example, require low haze ($< 3\%$) to avoid blurred viewing of the display.^{13,24} On the contrary, electrodes with high haze may enhance the performance of solar cells: greater scattering of the incoming photons increases their optical path length and thus the probability of absorption, which is important especially for thin film solar cells.^{25–27}
- The mechanical **flexibility**, which has recently become important and is challenging the state-of-the art materials (see section 2.1.4). The trend for novel flexible devices on polymer substrates requires electrodes with high electrical stability upon bending and folding to turn visions like rollable displays or wearable solar cells into reality. While electrical resistance and optical transmittance are well defined parameters and standardized test methods are available, there is no standard for measuring the bending stability of TEs (yet). Most commonly used in scientific publications is the relative change in resistance $(R-R_0)/R_0$ as a function of bending cycles. The bending radius is usually chosen between 1–20 mm. Many publications also report the change in resistance as a function of the bending radius. The specific requirements again strongly depend on the application.
- The **surface roughness**: In particular for multilayer thin film devices like OLEDs and OSCs, the surface roughness must be below the thickness of a typical active layer (often ~ 50 -100 nm) to avoid short circuiting of the device.^{28,29}
- The **work function** of the layers (important for OLEDs and solar cells).²
- The **adhesion** of the film to the substrate.³⁰
- The electrical **long-term stability** with humidity and temperature.¹⁴

^a According to ASTM D1003, the haze of a material is defined as the fraction of light that is scattered at angles greater than 2.5° in forward direction.

2.1.2 Transparency-conductivity trade-off

The **conductivity** σ of solid materials can be described in first approach by the Drude model^a:

$$\sigma = en\mu = e^2\tau \cdot \frac{n}{m^*}$$

with e the elementary charge, n the carrier concentration, μ the carrier mobility, τ the scattering time (time between scattering events), and m^* the effective carrier mass.³¹ To obtain high conductivity, high carrier concentrations n and/or high carrier mobility (high scattering time τ and low effective mass m^*) are required.³

The **optical behavior** is determined by two barriers: the free carrier reflection edge (represented by the plasma energy) and absorption by interband transitions (represented by the band gap).³²

The free carrier reflection edge depends on the plasma energy

$$E_p = \frac{h}{2\pi} \cdot \omega_p$$

with h the Planck constant and ω_p the plasma frequency, which is defined by

$$\omega_p^2 = \frac{e^2}{\epsilon_0\epsilon_r} \cdot \frac{n}{m^*}$$

with ϵ_0 and ϵ_r the vacuum and relative permittivity.³ At frequencies below ω_p , delocalized electrons screen the electric field of the incoming light and reflect it; at frequencies above ω_p , light is transmitted because the electrons cannot follow the oscillation of the incident electromagnetic wave.³³ To obtain transparency in the visible range, the plasma energy should be minimized (at least to below the visible spectrum, < 1.75 eV). Hence, n should be small and/or m^* large.

Photon absorption by interband transitions can further influence the optical response of materials in the visible range. Gold and copper, for instance, have interband transitions

^a Drude initially proposed the model to describe the electrical transport in metals. Free (valence) electrons move randomly inside the crystal (no net velocity). Under the influence of an external electrical field, the electrons get accelerated until they collide with the positive lattice ions or lattice defects (described by the scattering time). The theory has been extended by Lorentz (Drude-Lorentz model) and later by Sommerfeld and Bethe including quantum mechanics (Drude-Sommerfeld model).

with energies in the visible spectrum that cause the characteristic coloring. In semiconductors with high energy band gaps (> 3 eV) interband transitions occur above the visible spectrum.³⁴

In summary, the ratio of the carrier concentration and the carrier effective mass (n/m^*) is the key factor for the design of transparent conductors, which simultaneously reveals the **trade-off** between conductivity (n/m^* should be maximized) and transparency (n/m^* should be minimized)^a: high carrier concentrations and low effective carrier mass required for high conductivity will shift the free carrier reflection edge into the visible range and thus cause reflectivity of the material.³² Metals, the best electrical conductors, have high carrier concentrations ($n \gg 10^{22}$ cm⁻³) and thus a plasma edge in the deep-UV spectral range.^b A successful strategy for TE design is to use materials with limited carrier concentrations, but increase the mobility of the charge carriers (see next section).³

2.1.3 Transparent conductive oxides

Transparent conductive oxides (TCOs) were the first TE-materials applied in optoelectronic devices and are still major players in the field of TEs.³ Their unique balance of transparency and conductivity follows from wide-bandgap n-type semiconductors with low electron effective mass (In₂O₃, ZnO, SnO₂) doped to increase carrier concentration.^{3,34} The high energy band gap ensures that absorption by interband transitions is shifted above the visible spectrum (> 3 eV). The intrinsically low carrier concentration can be increased by doping, limited by the dopant's solubility in the host material.^c As the attainable carrier concentrations are still relatively low compared to metals (about a factor of 50-100), the plasma energy is still far below the visible spectrum and light is transmitted in this wavelength range.³ The limited carrier concentration requires high mobility of the charge carriers to obtain high conductivity. The mobility $\mu = e\tau/m^*$ is

^a Precisely only holds for homogeneous materials.

^b Recently, Zhang et al. reported transparent conductors based on correlated metals, which combine high carrier concentrations with low plasma energies because strong electron-electron interactions result in a high effective electron mass.³²

^c Doping of the host material also influences the width of the band gap.^{202,203} Two mechanisms compete: (1) band gap widening by the Burstein-Moss effect: doping leads to population of states within the conduction band, which increases the Fermi level. (2) band gap narrowing by many-body effects: electron-electron scattering and electron-impurity scattering causes valence and conduction band to shift. For doped In₂O₃, the interplay of both mechanisms result in a net increase of the gap.²⁰³

determined by the scattering time τ (should be maximized) and effective carrier mass m^* (should be minimized). The scattering time is intrinsically limited by scattering at ionized impurities caused by the dopant. Additional scattering at crystallographic defects (dislocations, grain boundaries, etc.) can be reduced by appropriate deposition and annealing. Thus, high-temperature post-processing steps are often necessary for TCOs with high-end performance.^{34,35} The second important parameter is the effective mass, which should be reduced to increase mobility^a. In particular, oxides of the post-transition metal cations (“TCO cations”) Zn^{2+} , Cd^{2+} , In^{3+} , Sn^{4+} show small electron effective masses as their overlapping s-orbitals form broadly dispersed conduction bands.^{3,36,37} $\text{ZnO}:\text{Al}^+$, $\text{SnO}_2:\text{F}^+/\text{Sb}^+$, and $\text{In}_2\text{O}_3:\text{Sn}$ (ITO) are the most prominent materials owing to their large bandgap (> 3 eV) enabling the use in the visible and near-infrared (NIR) range.³ Among all, ITO shows the best performance and has been almost exclusively used in optoelectronic devices; mobilities up to $100 \text{ cm}^2\text{V}^{-1}\text{s}^{-1}$ result in resistivities down to $1\text{-}2 \cdot 10^{-4} \Omega \cdot \text{cm}$.³ Sputtered ITO coatings (on glass) usually have a transmittance about 90% at a sheet resistance $\geq 10 \Omega/\text{sq}$, which serves as benchmark for new technologies (see next section).^{5,35,38}

2.1.4 Solution-based transparent electrodes for flexible devices

Though still more than 90% of the entire TE market is dominated by ITO, several limitations and undesirable properties have led to a copious research interest to replace ITO in the last decade.^{2,39} Commonly stated motivations include the scarcity of indium and the accompanying high raw material price; the concentration of production to few countries (China, Japan, Canada, etc.) and the concomitant strategic dependence further motivated the search for alternatives (particularly in Europe and the United States). Limited resources of indium certainly conflict with the strongly increasing demand for optoelectronic devices, but it should be noted that the cost of raw indium constitutes only 2% of the total costs for ITO production. The major cost drivers are the slow and inefficient^b sputter process in vacuum and subsequent high-temperature post-processing steps required for high-grade ITO (see section 2.1.3).^{34,35}

^a As n is still rather low, a decrease in m^* (thus, an increase in n/m^*) can be tolerated without shifting the plasma energy in the visible range.³⁶

^b Large fractions of the sputtered target end up at the walls of the chamber.⁵

Nevertheless, cost arguments (raw material prices, process costs) are always subject to fluctuations and should not be considered a single exclusion criterion. Raw indium prices have significantly fallen in the last 2 years and leading ITO suppliers have recently slashed their prices, which is impeding the replacement of ITO in established devices and processes.^{40,41}

Novel flexible devices based on polymer substrates entail new requirements that significantly impede (if not exclude) the use of ITO: (1) ITO shows only limited bendability due to its ceramic brittleness. Cracks form already at low strains and lead to a sharp increase in resistance. (2) High-grade ITO requires processing at elevated temperatures exceeding the thermal budget of many polymer foils.^{3,5,34,35}

Hence, new materials with optoelectronics properties comparable to ITO ($T \geq 90\%$, $R_s \leq 10 \Omega/\text{sq}$) that can be processed at low temperatures and are flexible enough to withstand repeated bending cycles at low bending radii have been the focus of intense research in the last decade. The search for ITO replacement materials has been accompanied by the wish to replace vacuum technology as a major cost driver by solution-phase processing. Solution-phase processing has the potential to coat large areas (several meters wide) at high speeds (up to 100 m/min), while having lower capital and maintenance costs than vacuum processing.^{5,42} The following sections will solely focus on alternatives that can be coated from solution.

Conductive polymers were among the first alternatives in the late 20th century.² Polymers can be coated from solution and are mostly flexible. The prevalent polymers are polythiophene derivatives like PEDOT:PSS^a, which is often used as hole injection layer for OLEDs.^{43,44} High optical transmittance ($T > 90\%$) can be obtained, but relatively high sheet resistances ($R_s > 100 \Omega/\text{sq}$) and limited stability under exposure to high temperature, humidity, and UV radiation impede the use of conductive polymers in certain applications.^{5,45,46}

The second major class comprises carbon materials, including **carbon nanotubes (CNTs)** and graphene. CNTs have been considered a promising alternative since their discovery in the 1990's because of their outstanding electrical properties: individual

^a poly(3,4-ethylenedioxythiophene) poly(styrenesulfonate)

CNTs have high carrier mobilities exceeding $100\,000\text{ cm}^2/\text{Vs}$ and can reach conductivities up to $200\,000\text{ S/cm}$.² Transparent films were fabricated from CNT inks by solution-based deposition processes including spray coating⁴⁷, Meyer rod coating⁴⁸, and dip coating.⁴⁹ The expectations on CNT-based TEs were reduced by the difficulty to achieve CNTs with high purity in large amounts and the limited conductivity of CNT thin films due to large contact resistances between the individual CNTs.²

Considered the “rising star” in materials science, **graphene** is a promising candidate for transparent electronics, too, based on its outstanding electrical (ultrahigh mobilities) and optical (only 2.3% loss in transmittance per single layer) properties.^{50,51} However, TEs from solution-processable inks based on graphene flakes underperformed the theoretical expectations facing the same problem of large contact resistances as observed for CNT inks.² High-end TEs were reported only by chemical vapor deposition (CVD).^{51–55}

Metals, the best electrical conductors, are opaque in bulk: high carrier concentrations, which enable the superior electron transport, imply high reflectivity in the visible range (see section 2.1.2). Metal films can become optically transparent when they are thin (usually less than 10 nm), but discontinuous growth impedes the fabrication of such layers and electron surface scattering will limit the electrical conductivity at this thickness.^{2,56} A second strategy can overcome these limitations: use thin metal (nano)structures that carry the electrical current but are sufficiently small to avoid strong light scattering in the visible range and separate them by voids that account for the transmission of light. The transparency/conductivity ratio depends on the area fraction that is covered by the material. First approaches included metal microgrids based on “top-down” vacuum processing. Today, “bottom-up” approaches where metal nanostructures are deposited from liquid dispersions reduce the required amount of material and simplify the deposition process.⁴ Two main classes can be distinguished: **random nanowire networks** (section 2.1.4.1) and **ordered metal grids** (section 2.1.4.2).

2.1.4.1 Random metal nanowire networks

Solution-phase synthesized metal nanowires with diameters between 20-150 nm and lengths of 50-200 μm are dispensed onto a substrate in a random arrangement. At certain area fraction, the interconnected wires percolate and form a continuous electrical

pathway. For applications as TEs, nanowire densities above the percolation threshold are required.⁵

The optoelectronic properties of the layers are primarily set by the area fraction

$$AF = N \cdot L \cdot D$$

with N the number of nanowires per unit area, the wire length L , and the diameter D .⁵ The transmittance of random networks can be estimated by

$$T = e^{-AF \cdot \frac{C_{ext}}{L \cdot D}}$$

with the extinction cross-section C_{ext} that is the amount of light absorbed and scattered by a single nanowire.⁵

The resistance for N above percolation can be estimated in first approximation by

$$R_s = \frac{\rho_\infty \cdot \rho_{NW}}{m/A}$$

where ρ_∞ ($\Omega \cdot m$) is the bulk resistivity of the material, ρ_{NW} ($kg \cdot m^{-3}$) is the nanowire density in the film, and m/A ($kg \cdot m^{-2}$) is the mass of the nanowires per unit area.⁵ The equation, however, disregards two fundamental characteristics of nanowire networks: (1) The resistivity of a nanowire is always higher than the bulk resistivity due to electron surface scattering.⁵⁶ (2) Contact resistances between the individual wires play a major role and determine the overall sheet resistance of the film.^{57,58} After synthesis, nanowires are typically surrounded by a polymeric ligand shell (e.g. polyvinylpyrrolidone (PVP)) that stabilizes the wires in solution, but provokes high resistances at the wire-wire junction.⁵⁷ Two complimentary approaches can be applied to improve the overall conductivity of a metal nanowire network: reduce number of interfaces or reduce electron barrier at the interfaces. At a fixed area fraction, increasing wire length will reduce the number of interfaces for a given distance, which motivates the use of ultrahigh aspect ratio wires.⁵⁸ In contrast to carbon materials (see section 2.1.4), metal nanostructures can be welded together by a sintering treatment. Removal of ligands and subsequent formation of direct metal-metal contact significantly reduces the contact resistances (see also section 2.3).

The best-studied wire-based TEs are **silver nanowires (AgNWs)**. During the last 5-10 years, a large number of articles has been published on AgNW networks and even vast amounts of reviews exist^{a,5,13,38}. Various wet-coating methods have successfully been applied to fabricate TEs based on AgNW networks, including drop casting,⁵⁹ spray-coating,⁶⁰ rod-coating,⁶¹ spin-coating,⁶² and vacuum filtration with subsequent transfer.^{63,64} Large-area TEs with optoelectronic properties comparable to ITO ($T > 90\%$, $R_s < 10 \Omega/\text{sq}$) but with superior mechanical flexibility were reported in literature. Several companies were founded (many as university spin-offs) focusing on synthesis and/or application of AgNWs including *BlueNano*, *Seashell technologies*, *Cambrios*, *C3Nano*, among others.

Second major player are **copper nanowires (CuNWs)**.⁶⁵⁻⁶⁷ Copper is 6% less conductive than silver, but 1000 times more abundant and significantly cheaper. TEs of CuNWs with comparable properties to AgNW networks and ITO have been reported in literature, but copper's high susceptibility to oxidize limits the long-time stability of CuNW films. Novel approaches are trying to circumvent this drawback by overgrowing the copper core with oxidation-resistant metals, for instance.^{65,68}

Although random nanowire networks are close to application, there is still no commercial breakthrough.⁶⁹ Apart from business arguments, several technological issues may cause the sluggish replacement of ITO:

- Random deposition allows only for limited control of the network geometry. The nanowire density can be tuned, but not the position of individual wires.
- Haze values of several % impedes the use in high-end touch screens.^{13,70}
- High surface roughness of the loose nanowire networks challenges the fabrication of multilayer thin-film devices like OLEDs.²⁹ Recent studies reported ultra-smooth AgNW films by mechanical pressing or polymer coating.^{29,59,61}

2.1.4.2 Ordered metal grids

Grids with controlled geometry have shown the potential to outperform ITO with regard to electro-optical properties and mechanical flexibility.⁷¹ Several advantages over random nanowire networks exist: Control over the grid's microstructure enables the specif-

^a Literature search on web of science (accessed Feb 20th 2017) yielded 567 publications and 15407 citations for the combination "silver nanowire AND transparent electrode".

ic tuning of the properties for a particular application. Material is only placed where it is needed; no isolated wires or dangling wire parts exist that reduce transmittance but do not actively take part in the current transport.⁷²

The **main parameters** affecting the grid properties are the linewidth w , the pitch p , the line height h , and the grid shape (see Figure 2). Linewidth and pitch of the grid determine the ratio between optical transmittance and electrical conductivity and have to be mutually adjusted according to the desired properties: increasing the linewidth and/or decreasing the pitch will increase the conductivity, but decrease optical transmittance, and vice versa.^{73,74} Increasing the line height lowers the resistance, but keeps the transmittance largely unaffected and is thus an efficient way to reduce the trade-off between transparency and conductivity.^{75,76} The grid geometry can affect the device performance, too (see below); common designs for TEs include linear, square, hexagonal, or triangular grids.

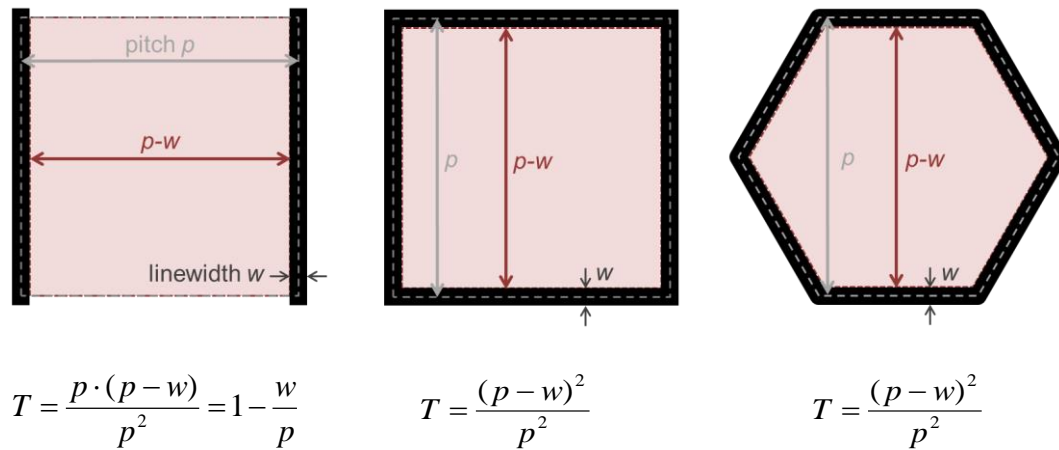


Figure 2: Top view of the unit cells of ordered grids with (a) linear, (b) square, and (c) hexagonal geometry and corresponding equations to calculate the optical transmittance T considering the clear aperture, where w is the linewidth and p the pitch of the grid.

The **optical transmittance** of grid structures can be approximated considering the clear aperture of the grid, which is defined as the area not covered by material.^{77,78} Figure 2 gives an overview of the three major grid designs (lines, squares, and hexagons) and the corresponding equations to calculate the theoretical transmittance based on the clear aperture.

The clear aperture serves as a good approximation of the grid's transmittance, but neglects the influence of light scattering and plasmonic effects.^{77,79} For instance, grids with sub-wavelength structures can have complex optical responses; strong coupling of

surface plasmons in nanohole meshes has been reported to induce extraordinary transmission, for example.^{80,81}

The **sheet resistance** of a metal grid can be estimated using Kirchhoff's law.⁷⁷ For a square nanowire network, the sheet resistance is

$$R_s = \frac{N}{N+1} R_{wire} = \frac{N}{N+1} \frac{\rho \cdot L}{w \cdot h}$$

with the resistivity ρ , the wire length L (equals the network pitch p), the linewidth w , and the line height h . For large networks, the first term is close to unity, which leads to (with $L = p$):

$$R_s \approx \frac{\rho \cdot p}{w \cdot h}$$

The ratio between transparency and resistance is not the only factor affecting device performance. For instance, Neyts et al. studied the voltage loss in metallic grids used for OLEDs with different shapes (triangular, square, or hexagonal).⁷³ Grids with identical conductivity and transmittance were shown to have different voltage losses for different geometries: a hexagonal mesh had 6% lower loss than a square grid. Solar cell performance has been reported to depend on the geometry of grid-based TEs, too.^{82,83} The influence of grid geometry on device performance underlines the superiority of grids with controlled and tunable geometry over random meshes.

The fabrication of ordered metal grids started with established “top-down” processes: lithographically prepared grids served as mask for subsequent metal evaporation. The number of processing steps, waste of excess material, and complex vacuum technology limit the cost-efficiency of this technology. In recent years, “bottom-up” processes that additively deposit material from liquid dispersions have been shown to increase structural flexibility, reduce complexity, require fewer processing steps, and reduce the waste of material (see next section).⁴

2.2 Patterning of nanoparticle inks for electronics

A variety of technologies has been used to print defined structures from liquid inks containing nanomaterials.³⁹ Metal nanoparticle inks are usually dispersions of nanoparticles with diameters below 100 nm and a metal content between 10 and 70%.⁸⁴ The liquid phase is usually a mixture of multiple solvents to adjust wetting, evaporation, etc.^{30,66} In the following section, the most relevant techniques for the fabrication of ordered transparent metal grids will be discussed. Section 2.2.2 will introduce the novel concept of direct nanoimprinting for high-resolution patterning of nanoparticle inks.

2.2.1 Fabrication of transparent metal grids from nanoparticle inks

Ahn et al. introduced the concept of **direct writing** of nanoparticle inks.⁸⁵ A concentrated silver nanoparticle ink (mean particle size: 20 ± 5 nm; solid content: 78 wt%) was extruded through a tapered cylindrical nozzle that was translated using a three-axis robotic motion stage. Square silver grids with a linewidth of 9 μm and height of 3 μm were prepared with a varying pitch from 100-400 μm . Thermal annealing at 200°C for 2 h after printing yielded grids with resistivities down to $3.64\cdot 10^{-5}$ $\Omega\cdot\text{cm}$. Grids with a pitch of 400 μm showed a transmittance of 94.1%.

Electrohydrodynamic (EHD) jet printing increases the resolution of inkjet printing.^{86,87} Droplets much smaller than the actual nozzle diameter can be ejected by applying a high electric field that stretches out the meniscus on the tip of the nozzle. Jang et al. used a commercial silver ink (ENJET; solid content: 70 wt%) to print grids with a linewidth of 7.53 μm , a height of 1.46 μm and a pitch between 50-300 μm from a nozzle with an inner diameter of 100 μm . Grids with 150 μm pitch had an optical transmittance of 81.75% and a sheet resistance of 4.87 Ω/sq after annealing at 200°C under near-infrared light.⁸⁶ Schneider et al. increased the resolution of the method in a process called **NanoDrip printing** (droplet diameter: < 100 nm; nozzle diameter: 1 μm).⁸⁸ They printed silver and gold nanogrids from commercial nanoparticle inks with linewidths from 80 to 500 nm, heights between 200 nm and 1.5 μm , and pitches of 10-20 μm . The grids exhibited superior optoelectrical properties ($R_s = 8\text{-}20$ Ω/sq , $T = 94\text{-}97\%$) after thermal annealing at 150-250°C at low printing speeds of ~ 30 min for the patterning of 100 μm^2 .

The fabrication of grids by **laser sintering** was introduced by Hong et al.⁸⁹ and Lee et al.⁹⁰. Both fabricated transparent metallic grids on flexible substrates using selective laser sintering of metal nanoparticle inks. Nanoparticles in suspension were first spin-coated onto a substrate. A focused laser acted as local heat source sintering the particles selectively to conductive microlines. Patterning and sintering were performed in a single step (see also section 2.3.1). The applied laser power determined the temperature distribution and thus, the structure of the sintered lines. Unsintered particles were removed by a subsequent washing step. The resulting grids showed high transmittance (> 85%) and low sheet resistance (30 Ω /sq). Laser sintering, as maskless direct writing methods, allows for the fabrication of arbitrary structures and flexibility of the process. Drawbacks of the method are limited resolution (linewidth 10-30 μ m) and waste of the unsintered parts of the ink layer.

Layani et al. introduced a printing process based on the combination of **inkjet printing** and the **coffee ring effect**.⁹¹ Particles inside sessile suspension droplets are known to assemble at the perimeter of the contact line upon evaporation if it is pinned, well-known as coffee ring effect.⁹² Layani et al. ink-jetted drops of a silver nanoparticle ink (mean particle diameter: 20 nm; solid content; 0.5 wt%) in a 2D-array. The particles assembled into dense interconnecting metallic rings that had a linewidth of 10 μ m, a height < 300 nm, and a “hole” of 150 μ m in average.⁹¹ The process yielded TEs with a transmittance of 95% and a sheet resistance of 4 Ω /sq after annealing in HCl vapor (see also section 2.3.2). The concept was extended by Zhang et al. who ink-jetted linear liquid patterns (arrays of drops) of a silver nanoparticle ink.^{93,94} Upon evaporation, the silver nanoparticles aggregated at the three-phase contact line and formed two parallel lines. The distance between two parallel lines was 60–80 μ m and the distance between each set of double lines was set to 800-900 μ m. They achieved square grids with a linewidth of 5-6 μ m and a height of 0.3-0.4 μ m on hydrophilic glass substrates. The resulting grid had a transmittance of 93.6% and a sheet resistance of 30 Ω /sq.

Higashitani et al. described a process named “**evaporative lithography**” yielding ordered metal grids based on AuNPs by templated evaporation.⁹⁵ A gold nanoparticle dispersion (mean particle diameter: 10 nm; solid content: 2 wt%) was dropped on a stainless steel mesh that had been placed on top of a plasma-treated glass substrate. The solution spread over both, mesh and glass substrate. During evaporation, the liquid flowed

towards the bars of the steel mesh, forming a grid with open spaces. After drying, the steel mesh was removed to obtain gold grids with a linewidth of 4 μm , a height of 80 nm, and a pitch of 100 μm . Sintering at 425°C for 20 min was necessary to remove the organic ligands and to turn the grid conductive. The resulting grids showed transmittance of 82% at a sheet resistance of 20 Ω/sq . Layani et al. extended the method to heat-sensitive substrates using metallic nanoparticle inks that can be sintered at room-temperature.⁹⁶ Silver nanoparticles with polyacrylic acid as electro-steric stabilizer coagulated when exposed to HCl vapors (see section 2.3.2).⁹⁷ The grids had an average linewidth of 5.7 μm , a height of 1.1 μm , and a pitch of 50 μm . The optical transmittance was 77% at a sheet resistance of 9 Ω/sq .

The concept of **flow coating** is based on the convective assembly of nanoparticles into dense lines: a droplet of the nanoparticle dispersion is confined between an angled plate and the substrate by capillary forces and forms a meniscus. Analogue to the coffee ring effect described above, solvent evaporation at the three-phase contact line induces a convective flux of solvent from the droplet that carries the nanoparticles to the contact line, where they get deposited on the substrate.⁹⁸ Linear movement of the plate stretches the meniscus until the contact line slips to a new position. Repeated movement of the plate after certain waiting times creates dense lines with defined spacing.⁹⁹ Park et al. reported the fabrication of transparent metallic grids by flow-coating of silver nanoparticles.¹⁰⁰ They prepared square grids with a linewidth of 7-10 μm , a height of 60 nm, and a pitch of 200 μm . The grids had optical transmittances between 70-88% at sheet resistances in the range of 132-332 Ω/sq . Flow coating is a simple method and does not require a complex printing setup, but is limited regarding grid geometry. On unpatterned surfaces, only straight lines (parallel to the meniscus) can be prepared; interconnecting grids (like the square grids reported by Park et al.) require two step processing.

In **nanosphere lithography**, monolayers of polystyrene (PS) spheres serve as mask for the fabrication of honeycomb meshes by deposition of material in the gaps between the spheres, first with material deposition based on evaporation.^{101,102} Kwon et al. were the first to report a fully solution-based process.^{103,104} They prepared silver meshes by coating a monolayer of PS spheres with a commercial silver ink (TEC-IJ-010, Inktec; solid content: 11.5 wt%) using a Meyer rod. After curing the ink (5 min at 100°C then 10 min at 140°C), the PS spheres were removed by sonication yielding conductive honeycomb

meshes with linewidths between 0.03-0.5 μm , a height of 70-200 nm, and a pitch that was dependent on the sphere diameter (600 nm, 3 μm , and 10 μm). Parasitic islands that degraded the transmittance near the mesh lines were eliminated by wet etching. The meshes had transmittances between 35-88% and sheet resistances ranging from 20 to 2000 Ω/sq .

Limitations

The described methods suffer from two common drawbacks: limited resolution and the need for sintering at elevated temperatures.

Metal lines with several micrometer width do not guarantee the invisibility of the grid, which limits the applicability as front electrode of displays, for example. The limited resolution requires large separation of the lines (large pitch) to achieve high optical transmittance. TEs with such large non-conductive holes do not perform well with devices like OSCs or OLEDs.^{5,73,105} Surface roughnesses in the micrometer range make thick metal grids incompatible with multilayer thin-film devices like OSCs or OLEDs. The need for smaller linewidths has been pointed out by IDTechEx^a as a major issue: “The battle between metal mesh suppliers will be fought on narrowing the linewidth and improving throughput and yield (biggest cost unknown/driver).”¹⁰⁶

In many cases, high temperature sintering is necessary to obtain low resistivity, which exceeds the thermal budget of many polymer substrates and thus impedes the use of such metal grids in the fabrication of modern flexible devices. Section 2.3 will discuss the effects of sintering treatments on nanoparticle inks and present novel sintering techniques.

2.2.2 Direct nanoimprinting of nanoparticles

Nanoimprint lithography (NIL) has become a powerful alternative to photolithography for patterning materials with high resolutions (down to nm) at high throughput and low costs.^{107,108} While in photolithography photons induce the patterning (e.g. develop photo resist), NIL relies on direct mechanical deformation that does not have diffraction limitations. A pre-patterned template, usually referred to as “stamp” or “mold”, is pressed into material and replicates the patterns of the stamp.¹⁰⁹ Many different types of

^a IDTechEx provides market research and business intelligence with a strong focus on novel technologies including Printed Electronics, 3D printing, RFID, wearables, etc.

nanoimprint lithography have been developed over the years, some with resolutions in the nanometer range and a vast field of applications.¹¹⁰ Usually, a thin polymer film or resist is patterned, which is either directly used as a material (e.g. as diffraction gratings or microfluidic devices) or serves as a mask for further processing steps like wet etching or metal evaporation, for instance. To ensure a complete filling of the mold and a high fidelity of pattern replication, the viscosity and surface tension of the imprinted material need to be considered.¹⁰⁹ The mold materials are usually classified regarding their Young's modulus (E):¹¹¹

- rigid molds ($E > \text{few GPa}$): silicon, SiO₂, glass, silicon nitride, nickel
- soft molds ($E < \text{few MPa}$): PDMS, polyurethane
- rigiflex molds ($\text{few MPa} < E < \text{few GPa}$): fluoropolymers

In conventional NIL, the stamp is placed in full contact with the substrate to imprint the pattern (batch process), which limits the application for large-area patterning: large contact areas require very large forces for high-resolution patterning; high adhesion forces impede the stamp release without pattern destruction. In addition, long processing times (few min or longer per wafer) interfere with the demand of high-throughput for practical applications. For high-resolution and high-throughput patterning, the group of L. Jay Guo investigated the transfer of NIL to roll-to-roll (R2R) processing.¹¹²⁻¹¹⁴ They attached the stamp (flexible or rigiflex) onto a cylindrical roller and incorporated it into a R2R setup enabling the imprinting of foils. As the effective imprinting area (contact line transverse to web moving direction) is small, less force is necessary for successful patterning and reduced adhesion forces facilitate the stamp release. Today, first commercial R2R-NIL systems are available.¹¹⁵

The use of elastomers has several advantages over rigid molds: elastomers can make conformal contact with substrates and allow for an easy release from rigid masters, even for complex structures. The beneficial properties provoked the development of several unconventional printing methods based on soft molds, grouped under the term “**soft lithography**”.^{116,117} Soft lithography generates patterns with feature sizes between 30 nm and 100 μm by pre-patterned elastomeric stamps. The most commonly used stamp materials are polydimethylsiloxanes (e.g. Sylgard 184) that has a low interfacial free energy ($\sim 21.6 \cdot 10^{-5}$ N/cm), good chemical stability, thermal stability, gas permeability, and optical transparency down to 300 nm.¹¹⁶ Stamp fabrication comprises the

molding of PDMS by drop-casting onto a master with relief structures (e.g. lithographically patterned silicon wafers or nickel shims), curing, and peeling off.¹¹⁸ **Micromolding in capillaries** (MIMIC) has been used for the patterning of nanoparticle inks. In MIMIC, a PDMS stamp is placed in contact with a planar substrate creating capillary channels by the grooves in the PDMS. A drop of the nanoparticle ink is placed at the ends of these channels. Capillary forces induce liquid filling of the cavities. After drying or curing of the material, the PDMS stamp can be removed. The method is applicable to a broad material range (liquid resist, nanoparticle solution, etc.) and enables the fabrication of features in the sub-100 nm scale.^{119,120} Duan et al. reported the fabrication of thin metal lines and grids (feature size down to 40 nm) by molding of gold nanoparticles (mean diameter: 3.5 nm).¹²¹ The capillary filling, efficient and fast over short distances, is significantly slowed down with increasing distance due to viscous drag of the liquid, which impedes the fabrication of large-area TEs.¹²² Small cross-sectional areas, required for high resolution, will further reduce the filling rate.¹¹⁹

In 2007, Ko et al. pioneered a process to fabricate metal structures with high resolution that combines elements of classical nanoimprinting and soft lithography using nanoparticle inks.¹²³ The process is based on **direct nanoimprinting of a nanoparticle ink** by a pre-patterned PDMS stamp and the subsequent sintering of the nanoparticles to a bulk material. Direct patterning eliminates the need for intermediate mask steps and requires only moderate temperatures and contact forces. The process consisted of several steps: AuNPs (mean particle size: 1-3 nm; ligand: hexane thiol) were dispersed in α -terpineol and dispensed onto a silicon substrate. A pre-patterned PDMS stamp was pressed into the solution under the pressure of 5 psi (~ 0.35 bar) at 80°C; nanoparticles filled the cavities, replicating the structure of the stamp. After solvent evaporation, the stamp was removed and the particles were sintered on a hot plate at 140°C. The temperature during printing affected the viscosity of the NP solution and had to be balanced for optimal printing results: increased temperature decreased the viscosity of the solvent; at the same time, increased temperature accelerated solvent evaporation and thus increased viscosity. Ko et al. successfully printed test structures (lines, dots, etc.) with high resolutions (feature size down to 100 nm) and tested the applicability of printed nanowire resistors in organic field effect transistors. Only small areas in the range of 30 μm were structured.

The work of Ko et al. was followed by many derived processes to fabricate **plasmonic metallic structures**. Liang et al. reported the fabrication of plasmonic metallic nanostructures in a similar process and studied the influence of printing temperature and pressure.¹²⁴ A temperature of 60°C was not sufficient to ensure complete filling of the cavities due to high viscosity; at 80°C, deformation of the stamp features was observed, which the authors attributed to accumulation of solvent vapor in the cavities. The applied pressure was adjusted between 3-6 bar: increasing the pressure decreased the amount of residual layer; at 6 bar, deformation of the stamp features led to poor pattern fidelity. Fafarman et al. prepared subwavelength arrays of nanopillars, nanowires, and nanoholes by direct nanoimprinting of a AuNP dispersion in hexane (mean particle diameter: 10 nm; particle concentration: 18 mg/mL).¹²⁵

Direct nanoimprinting of **electronic materials** has been largely restricted to the fabrication of electrodes for field-effect transistors (FETs). Park et al. reported printing of gold source-drain electrodes for OFETs on polyimide using the same protocol (AuNPs in α -terpineol; mean particle size: 1-3 nm; solid content: 10 wt%).¹²⁶ The average resistivity of the printed structures was $1.99 \cdot 10^{-7} \Omega \cdot \text{m}$, which is about 8 times the resistivity of bulk gold. Hu et al. extended the method to silver inks (AgNPs in α -terpineol; mean particle size: 10 nm, solid content: up to 15%). They fabricated organic FETs on flexible substrates using nanoimprinted silver electrodes and semiconducting polymers.¹²⁷ Yu et al. engineered the ligand shell of gold nanoparticles (mean particle diameter: 2.5 nm) to provide imprintability.¹²⁸ The ligand consisted of a thiol-group bonding to the gold surface, a stabilizing alkyl chain, and a tetra(ethylene glycol) segment with a cyclohexylammonium end-group that suppressed crystallization. In this way, they were able to print conductive patterns with feature sizes down to 40 nm without solvent or polymer additives.

In **summary**, direct nanoimprinting of colloidal nanoparticle dispersions is a suitable method to create metal structures with nm resolution at low processing temperatures ($\leq 80^\circ\text{C}$), compatible with flexible polymer substrates. The scalability of classical NIL suggests the potential of direct nanoimprinting to be transferred to large-area R2R processes, too. Successful application to large-scale electronics will greatly depend on the ability to ensure electrical connectivity over macroscopic distances. High pattern fidelity and percolation of the particles will be key aspects.

2.3 Sintering of nanoparticle inks for electronics

Electronic structures based on nanoparticle inks suffer from an inherent dilemma: ligand molecules on the particles' surface usually impede the electron transport between the particles and limit the conductivity of the printed features.¹²⁹ Nanoparticles from wet-chemical synthesis are usually capped by organic molecules (ligands) that tune the particle size and shape during synthesis and inhibit particle agglomeration in dispersion by electrostatic, steric, or electrosteric stabilization.¹³⁰ Conductive metal inks with high particle loads usually rely on steric stabilization by surfactant- or polymer-like amphiphilic organic molecules that bind to the nanoparticle surface via carboxyl, carbonyl, amine, or thiol moieties.^{30,84}

After deposition and drying of the ink, the organic stabilizers remain in the layer and act as dielectric tunneling barriers provoking high contact resistances at the particle-particle interfaces. To enable continuous electron transport between the particles, the insulating ligands have to be removed in a post-treatment. A common approach is to apply thermal energy by conventional methods like hot air in a convection oven or IR irradiation to decompose the organic material. Typical sintering temperatures are 150-350°C with processing times of 10-60 min.³⁰

Novel concepts of “sintering-free” inks with conductive ligand shells that render the sintering step obsolete are currently under scientific discussion, but only few publications exist. As an example, a novel sintering-free hybrid-ink has been developed by Reiser et al., co-authored by the author of this dissertation.¹³¹ Gold nanoparticles were capped with conjugated, electrically conductive polymers (PTEBS, PEDOT:PSS) that simultaneously provided colloidal stability and enabled electron transport from particle to particle. Printed lines were conductive (resistivity down to 0.04 Ω /sq/mil) after deposition without additional sintering.

Sintering of nanoparticle inks commonly occurs in two stages: (1) removal of ligands, (2) coalescence of the nanoparticles.⁸⁴ After ligand decomposition or detachment, unprotected particles coalesce by surface melting and diffusion of metal atoms from one NP to another (high surface mobility), driven by the reduction of the free surface energy.³⁰ The fusion of particles occurs at temperatures far below the melting point of bulk gold (1064°C), a phenomenon called “melting point depression”.¹³² Atoms at surfaces

have fewer bonds and thus lower cohesive energy than atoms in bulk; less energy is necessary to move them. Nanoscale objects have large surface-to-volume ratios, which increase with decreasing particle size and lead to a size-dependent melting point.^{133–135} Consequently, the required sintering temperature of small NPs is often set by the ligand removal rather than by the actual melting point of particles.

The high temperatures that are required to remove the stabilizers from NP inks (in the range of 150–400°C) require substrates like glass or silicon, but exclude most polymer substrates. Standard polymer foils have low thermal stability with glass transition temperatures on the order of 150°C; extended sintering at temperatures above will lead to severe foil deformation.⁸⁴ Novel sintering technologies should minimize the thermal impact on the substrate, but retain fast sintering for high throughput processing. Among many other publications, I would like to highlight the review of Schubert et al., which presents a good summary of novel concepts for sintering of NP inks.⁸⁴ Three of the most relevant technologies are based on photonic sintering (section 2.3.1), chemical sintering (section 2.3.2), and plasma sintering (section 2.3.3).

2.3.1 Photonic sintering

The basic idea of “photonic sintering” is to selectively heat the ink by the photothermal effect at wavelength where the ink has high absorption but the substrate has not. Metal nanoparticles commonly show strong surface plasmon resonances in the visible range, while substrate like glass and polymer absorb mostly in the UV range. Since the absorption characteristics change with the specification of the ink (base material, particle distribution, etc.), the process parameters (spectrum, power density) have to be adjusted for each system. Several technologies based on “photonic sintering” have been developed:

Near-infrared (NIR) sintering

Most polymers do not have strong absorbance in the NIR range (700–1500 nm). Irradiation in this wavelengths range will selectively sinter the ink and limit the energy input on the substrate minimizing substrate deformations.¹³⁶ NIR sintering is scalable and suitable for high-throughput R2R processing, commercial systems are readily available.¹³⁷ As the timescale of sintering is in the order of seconds, heat transfer from metal ink into substrate cannot be fully neglected, which makes NIR more suitable for substrates like paper than for ultrathin PET foil.⁸⁴ In the course of the process, the absorp-

tion behavior of the ink constantly changes as particle size and shape change upon sintering.⁸⁴ Hence, the sintering characteristics change and kinetics are often slowed-down.

Intense pulsed light (IPL) sintering

Continuous irradiation with light will heat up the particles, but the need to attain thermal equilibrium with the substrate will cause heat transfer to the substrate within milliseconds. Intense pulsed light with a pulse duration (t_{pulse}) much shorter than the time to achieve thermal equilibration between ink and substrate ($\tau_{\text{substrate}}$) heats the particles (by light absorption) locally before they can transfer the heat to the substrate.¹³⁸ For a homogeneous sintering, the pulse duration should be longer than the thermal equilibration time of the ink (τ_{ink}). While τ_{ink} is of the order of one microsecond or below, $\tau_{\text{substrate}}$ is at least several tens of milliseconds, which opens a window for the pulse duration ($\tau_{\text{ink}} < t_{\text{pulse}} < \tau_{\text{substrate}}$). The high energy density leads to locally high process temperatures, which reduces the processing time and thus increases throughput. Most commonly used are xenon stroboscope lamps with irradiation at wavelengths between 200 and 1200 nm. Appropriate conditions (pulse length, pulse intensity, flashing frequency, etc.) have to be chosen for each ink/substrate combination.⁸⁴

IPL treatment has been successfully used for sintering of copper inks^{139,140}, AgNWs^{141,142}, and silver inks.^{143,144} Several commercial systems are available from *Novacentrix* (Pulse Forge series) and *Heraeus noble light*.^{145,146}

Sintering by pulsed light is a cheap and energy efficient technique (30% of electrical energy converted into radiation, no complex optics necessary as for laser).¹⁴⁷ It is easily scalable and can be integrated into R2R systems.¹⁴⁸ For certain ink formulations, the high surface temperatures reached can lead to oxidation of the ink material under air; foil deformation has been observed after multiple flashing.¹⁴⁹

Laser sintering

Nanoparticles absorb the photons emitted from a laser, heat up by the photothermal effect, and sinter together. Controllable parameters are power output, writing velocity, wavelength, and operation mode (continuous wave or pulsed), which have to be chosen carefully to minimize the heat dissipation into the substrate material.

Ko et al. reported on the selective laser sintering of inkjet-printed microlines from gold nanoparticles.¹⁵⁰ The ink was dried and then locally sintered by scanning with a focused

Ar-ion laser (wavelength: 514.5 nm); unsintered nanoparticles were removed with organic solvents. Laser sintering can be used as a direct structuring method as well: metallic grid transparent conductors have been prepared by laser sintering of spin-coated particle suspensions on flexible substrates (see also section 2.2).^{89,90}

Laser sintering is versatile, arbitrary patterns can be sintered in a mask-less process. Locally high temperatures can cause damage to the substrate and to the ink (ablation of metal). Spot sizes of only a few mm leads to long processing times for large areas.

2.3.2 Chemical sintering

Chemical sintering involves the destabilization of the particle/ligand system by decomposition or exchange of the organic ligand molecules in the presence of a sintering agent.

One approach is the **chemical decomposition** of the ligands. Magdassi et al. showed that AgNPs capped with negatively charged poly(acrylic acid) (PAA) spontaneously coalesce when coming into contact with the oppositely charged polyelectrolytes poly(diallyldimethylammonium chloride) (PDAC).⁹⁷ The degree of coalescence can be tuned by the ratio between silver and PDAC. The PDAC was added by inkjet printing on top of the silver array. The process yielded highly conductive (5 times the resistivity of bulk silver) traces at room temperature, though many voids were present between the sintered zones. The Magdassi group further showed that PAA-stabilized AgNPs can undergo self-sintering in the presence of Cl^- ions as destabilizing agent.¹⁵¹ Cl^- ions replace the carboxylate anchoring groups of the PAA, which subsequently detaches from the nanoparticles' surface and enable particle coalescence at room temperature. NaCl solution or HCl vapor were applied as Cl^- source. Sintered lines had a resistivity of $3.84 \cdot 10^{-6} \Omega \cdot \text{cm}$ (~2.5 times the resistivity of bulk silver).

Other approaches involve the **exchange** of long stabilizing ligands by short ligands after layer deposition. Reduced inter-particle spacing eases the electron transport from particle to particle and enhances conductivity.^a Fafarman et al. reported the exchange of long-chain OAm ligands on AuNPs by the short inorganic ammonium thiocyanate (NH_4SCN).^{125,152} The resistance of spin-coated AuNP layers dropped by 10 orders of

^a The tunneling rate increases exponentially with decreasing separation between the NPs.¹²⁹

magnitude upon the ligand exchange. The layers were simply dipped into the thiocyanate solution (1 wt% NH_4SCN in acetone) after deposition.

Chemical sintering is often done at room temperature and minimizes the thermal input on ink and substrate, but compatibility of the substrates with the used solvents has to be guaranteed. Chemical reactions are often limited to specific ligand systems, which restricts the range of application. Post-treatment of printed layers in liquids can influence the stability of the layers; Fafarman et al. had to pre-coat the substrates by a mercaptopropyltrimethoxysilane (MPTS) layer to avoid particle desorption, for instance.¹²⁵

2.3.3 Plasma sintering

Ionized gasses formed by applying large energy (thermal, electric current or electromagnetic irradiation, etc.) are referred to as plasmas.⁸⁴ Plasma interacts with materials in several ways: highly reactive species (radicals, low-energy ions, and electrons) induce chemical reactions; the impingement of particles causes sputtering of the surface by momentum transfer and some heating of the material.¹⁵³ Together, they lead to the decomposition of organic material, e.g. by chain scission. The resulting low molar mass compounds are generally volatile and can be easily removed, especially at low pressures. Hence, plasma treatment is used as a standard method to remove organic residues from substrates.¹⁵³ Plasmas can be oxidizing (oxygen, air), reducing (hydrogen), or inert (noble gases, nitrogen). The ability to decompose organic material at low thermal budget makes plasma sintering an interesting approach to decompose and remove organic ligands.¹⁵⁴ The resulting highly reactive free metal surfaces can coalesce as described above without further temperature treatment.

Reinhold et al. treated inkjet-printed silver nanoparticle inks (roughly one micrometer thick) on common polymer foils by low-pressure argon plasma. Under the influence of the plasma, the silver particles coalesced into clusters as confirmed by XRD. The resistivity of the printed line was less than one order of magnitude above that of bulk silver.¹⁵⁵ Pronounced coalescence of the particles (as in the case of Reinhold) will destroy the nanoparticle size-dependent properties. Ozin and Cademartiri introduced a novel concept named “nanocrystal plasma polymerization” (NPP).¹⁵⁶ A soft, low-energy plasma treatment only partially removed the ligand shell while preserving the size-

dependent properties of the nanoparticles. An inorganic matrix connecting the particles enables the fabrication of mechanically stable and free-standing 3D architectures.

Plasma sintering has several advantages and disadvantages over traditional thermal sintering. Ligand decomposition does not require high temperatures, which limits the thermal budget of the method and makes it compatible with fragile substrates. The process is limited in depth by a phenomenon called “skin effect”: during plasma treatment a sintered top crust is formed, which prevents the plasma from penetrating the material. Depending on the choice of plasma, the treatment can be time-consuming (Reinhold reports treatment times of up to 1 h).¹⁵⁵ Long processing times will also affect the substrate, which can be detrimental for multilayer systems.¹⁵⁷

2.4 Ultrathin gold nanowires (AuNWs)

One-dimensional nanostructures (nanowires) with diameters in the nm range and aspect ratios (length to width) > 100 show prospects as nanoscale building blocks for “bottom-up” fabrication of electrical contacts in nanoelectronics.¹⁵⁸ Nanowires made from gold combine high electrical conductivity—gold is the third most conductive element after silver and copper—with superior chemical inertness. Various protocols have been reported for the synthesis of anisotropic gold nanostructures based on particle assembly¹⁵⁹, surfactant mediation^{160,161}, template assistance^{162,163}, or physical deposition.¹⁶⁴ The protocols generally yielded polycrystalline wires with diameters > 10 nm and high surface roughness. Since 2007, single crystalline gold wires with ultrathin diameter (between 1.6–2 nm) have become available from wet-chemical synthesis. The wires are grown along the $\langle 111 \rangle$ direction and exhibit ultra-high aspect ratios > 1000 (see Figure 3).

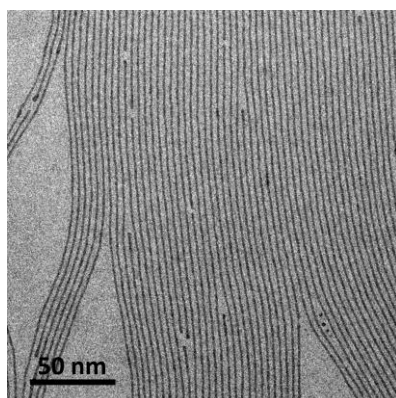


Figure 3: Transmission electron micrograph of as-synthesized AuNWs.

The next section will give an overview of the various protocols for the synthesis of ultrathin AuNWs and the hypothesis on their growth mechanism.

2.4.1 Synthesis and growth mechanism

Synthesis

The chapter of ultrathin AuNWs was opened with the first synthesis by Halder et al. in 2007.¹⁶⁵ Chloroauric acid ($\text{HAuCl}_4 \cdot 3\text{H}_2\text{O}$) was mixed with oleylamine and oleic acid in toluene to form in a first step gold nanoparticles with a diameter of around 2 nm. After the addition of ascorbic acid as reducing agent, the solution was aged for several hours to few days yielding wires with a diameter of around 2 nm and a length of about 1 μm .

In 2008, several papers on the synthesis ultrathin AuNWs were published in a very short time frame^a by groups around the major players in the field of colloidal nanomaterials.¹⁶⁶⁻¹⁶⁹ The synthetic protocols vary slightly, but follow the same concept: OAm acts as reducing agent and structure-directing agent at the same time. Because OAm is a liquid at room temperature it can be the solvent, too. The syntheses comprise the dissolution of chloroauric acid in OAm in the right stoichiometry and subsequent aging. As no additional reducing agent is used, the synthesis required long reaction times (4-5 days) and elevated temperatures (35-80°C). Only Lu et al. added AgNPs as reducing agent, but the reaction still required several days of ageing.¹⁶⁹ The protocols consistently yielded wires with diameters between 1.6-1.8 nm; only Wang et al. showed diameters between 3-9 nm.¹⁶⁶ The length of the wires was estimated to be in the range of 1-4 µm, although no direct experimental proof has been reported.

Feng et al. accelerated the reduction process by adding triisopropylsilane (TIPS) as additional reducing agent.¹⁷⁰ In their protocol, 3 mg HAuCl₄ were mixed with 100 mL OAm and 2.5 ml n-hexane, followed by the addition of 150 mL TIPS. The solution was kept undisturbed (no stirring) at room temperature for several hours until a gradual color change from yellow to dark red was observed. The protocol yielded wires with 1.8 nm in average diameter in a fast and robust synthesis and served as basis for many publications, including this thesis.

After synthesis, washing of the wires removes unreacted educts and excess oleylamine. Although slightly different protocols have been reported, the fundamental concept stays the same: addition of a polar solvent (usually ethanol or mixtures of ethanol and the respective solvent of the synthesis) induces agglomeration of the wires into macroscopic bundles, which precipitate (often assisted by centrifugation). After removal of the supernatant, the precipitated wires can be redispersed in the desired solvent; alkanes (hexane, octane, etc.), cycloalkanes (cyclohexane, cyclooctane, etc.), arenes (benzene, toluene), tetrahydrofurane (THF), and chloroform have been reported.

^a submitted between 6th and 30th of May 2008

Growth mechanism

The exact growth mechanism of AuNWs is still matter of scientific debate. Two main models are discussed (with several variations): “oriented attachment” and “micellar growth”. Both follow from the strong differences in the binding energy of OAm on different crystal facet of gold. Density functional theory (DFT) predicts an adsorption energy of amine groups on the {100} surfaces of a gold crystal that is roughly two times higher than on the {111} surfaces.^{171–173} Hence, OAm will preferentially adsorb onto {100} facets and preferentially be removed from {111} facets.

Halder et al. described the formation process of nanowires as “**oriented attachment**” of spherical particles.¹⁶⁵ The facet-dependent amine binding energy favors the fusion of two {111} facets and thus leads to anisotropic growth. After attachment, surface diffusion smoothens the particle junctions to a nearly circular wire cross section. Halder et al. based their theory on the fact that the final wire diameter is almost identical to the diameter of the nanospheres formed at the early stage of the synthesis and the fact that lattice defects (twin boundaries, stacking faults) can be observed in the nanowires.

Later publications explained the synthesis by a concept referred as “**micellar growth**”. Wang and Pazos-Pérez et al. proposed a mechanism similar to the reported mechanism for FePt nanowires: elongated inverse-micelle structures are formed by the self-assembly of OAm, within which elongated polyhedral gold nuclei are formed.^{166,168,174} Different OAm densities on the different crystal facets of the initial gold nuclei lead to directed growth into direction with low OAm packing density, $\langle 111 \rangle$ (see above).¹⁷⁴ Huo and Lu et al. proposed a slightly different mechanism.^{167,169} They believe that after partial reduction of Au^{3+} to Au^+ , Au^+ species is complexed by OAm to form ordered mesostructures due to strong interactions of the OAm side chains. Slow reduction of the gold ions inside the mesostructures results in anisotropic gold wires.

The growth mechanisms in the original publications on nanowire synthesis were merely based on theoretical assumptions and ex-situ TEM observations, Loubat et al. were the first to study the growth mechanism of AuNWs in-situ.¹⁷⁵ They used small-angle X-ray scattering (SAXS) to detect the fractions of spheres and wires during synthesis using a protocol by Feng et al. with modifications. They found that the volume fraction of spheres varied only slightly in the beginning of the synthesis and stayed almost constant

after 20 min, the time when first nanowires were detected. This is not expected for growth by oriented attachment, where spheres should be consumed during the formation process of the wires. They conclude that the concept of “micellar growth” is the prevalent mechanism underlying the anisotropic growth.

The theory of “micellar growth” has been further supported and extended by a recent theoretical study on the role of amine surfactants in the synthesis of anisotropic gold nanocrystals.¹⁷² You et al. studied the absorption characteristics of amine molecules (including OAm) on different facets of noble metals by MD simulations and DFT calculations and proposed a detailed growth mechanism of AuNWs. Their results indicate two major features of OAm affecting the anisotropic growth of gold nanocrystals: (1) Different adsorption energies cause different OAm packing densities on the {100} and {111} facets of gold crystals. (2) Strong interactions between the carbon-chains of self-assembled OAm molecules prevent the diffusion of metal ions through them and inhibit their subsequent incorporation into the nanocrystal. The efficiency of the blocking decreases with decreasing density of OAm molecules and thus changes with the different facets. Based on their observations, they proposed a multi-step growth mechanism of AuNWs: In a first step, the $\text{Au}^+/\text{Au}^{3+}$ -ion/OAm complex forms a micellar structure due to the self-assembly of OAm (see Huo and Lu et al.^{167,169}). Inside the micelles, Au ions are partially reduced to Au atoms that form a first nucleus. By addition of Au atoms, the nucleus grows into a nanocrystal (1-2 nm in diameter) bounded by {100} and {111} facets (see Halder¹⁶⁵, Wang¹⁶⁶ and Pazos-Pérez et al.¹⁶⁸). In a last step, the nanocrystals grow along the $\langle 111 \rangle$ direction yielding highly anisotropic nanowires.

At about the same time as You et al., the group of Peidong Yang published a high-resolution TEM (HRTEM) study of ultrathin AuNWs providing a detailed real space analysis of the wires' atomistic structure and growth.¹⁷⁶ They imaged single wires (synthesized according to the protocol of Feng et al.) by aberration-correction HRTEM and analyzed the stacking sequences of atomic planes. A large number of stacking faults suggested that beside the commonly accepted concept of “micellar growth”, oriented attachment can play a role in the wire formation, too: shorter nanowire may merge and form a single nanowire.

2.4.2 Self-assembly

First statements on the self-assembly of AuNWs were based on TEM observations. Halder and Feng et al. found closely packed bundles of parallel wires with a characteristic distance of around 2 nm after evaporation of a AuNW drop.^{165,170} Several groups reported the assembly of wires into monolayers at liquid-air interfaces. Sánchez-Iglesias et al. prepared densely aligned monolayers of AuNWs at a diethyleneglycol-air interface.¹⁷⁷ The wire arrays were transferred to glass substrates and showed an average interwire separation of around 3 nm. Depending on the functionality of the glass, the wires preserved the self-assembled structure (glass with hydrophobic coating) or grouped into larger bundles (unmodified glass). Chen et al. reported the formation of “giant superlattice nanomembranes” made of AuNWs.¹⁷⁸ AuNWs dispersed in chloroform were carefully spread onto a water surface in a Langmuir-Blodgett trough. Dense monolayers formed, which they attribute to strong hydrophobic interactions between OAm ligands.

Loubat et al. studied the self-assembly of AuNWs in liquid phase by SAXS.¹⁷⁵ They observed well-resolved Bragg peaks indicative of hexagonal nanowire superlattices few hours after synthesis. The lattice parameter was 9.7 ± 0.1 nm, which corresponds to an interwire distance of 8 nm considering a wire diameter of 1.7 nm. The interwire distance equals approximately four times the length of oleylamine (2.1 nm), which led to the model of a parallel assembly of wires separated by an oleylamine bilayer. The domain size was estimated to be around 70 nm based on the width of the Bragg peaks. An isotropic SAXS pattern indicated that the self-assembly occurs randomly in dispersion, which supports the theory of homogeneous nucleation of the self-assembly in liquid phase, rather than at the container's wall. The commonly reported wire-wire distance of 2-4 nm in case of dried AuNW thin films can be explained by an OAm monolayer on the wires' surface after washing and the partial interdigitation of the OAm alkane chains.¹⁷⁵

2.4.3 AuNWs for transparent electronics

Their self-assembly sets AuNWs apart from stiff AgNWs or CuNWs, which form networks resembling “pick-up sticks”. The ultrathin wires' high mechanical flexibility and their high aspect ratio enable the formation of line contacts between the wires. Multiva-

lent supramolecular interactions between the OAm ligand molecules lead to bundling of the wires upon drying rather than forming networks of interconnected single wires.¹⁷⁹

In 2014, the application of AuNWs for electronics was largely restricted to sensing. Wearable sensors from the group of Wenlong Chen were reported based on thick random AuNW films with sheet resistances in the M Ω range.^{180–182} Sánchez-Iglesias et al. were the first to report AuNWs for transparent electronics. They prepared thin films of densely aligned AuNWs by self-assembly at a liquid-air interface (see section 2.4.2).¹⁷⁷ The monolayers were manually transferred to glass substrates. The layers exhibited outstanding transmittance ($T = 96.5\%$), but the sheet resistances remained rather high ($R_s = 400 \Omega/\text{sq}$)^a. Limited stabilities of the layers at elevated temperatures (150°C, 1 h) were pointed out as a major drawback by the authors. Chen et al. fabricated AuNW mono- and multilayers by a Langmuir–Blodgett technique (see section 2.4.2).¹⁷⁸ Monolayers exhibited optical transmittances of up to $T = 97\%$ at sheet resistances of $R_s \sim 1.1 \text{ M}\Omega/\text{sq}$. Increasing the number of layers decreased sheet resistance at the price of reduced transmittance: for 10 layers, the transmittance dropped to $T = 37\%$, and the sheet resistance decreased by one order of magnitude.

The reported studies demonstrated AuNW layers with superior optical properties, but high sheet resistance and poor stability remained limiting. As-prepared AuNW films generally exhibit **high sheet resistance** (in the M Ω range) which is sufficient for sensing applications but impedes the use as TE, where tens of Ω/sq are required for reliable operation (see section 2.1.1). The limited conductivity of AuNW films can be attributed to two intrinsic effects: (1) The insulating OAm ligand shell impedes electron transport from wire to wire resulting in large contact resistances (see also section 2.3).^{178,183} (2) The ultrathin nature of the wires (only ~ 8 atoms in diameter) implies significant electron scattering at the nanowire surface as the wire diameter is significantly smaller than the mean-free pathlength of electrons in gold (around 40 nm).^{56,178,184}

Ultrathin gold nanowires are highly prone to fragmentation by the “**Plateau-Rayleigh instability**”^b. More than 150 years ago, Joseph Plateau predicted that liquid cylinders are unstable to radius perturbations with a wavelength larger than the circumference of

^a The sheet resistance was measured between evaporated gold electrodes with a very small spacing of only 100 μm . Sheet resistances of macroscopic areas were not reported.

^b Often named only “Rayleigh instability”.

the cylinder.¹⁸⁵ The cylinder will fragment into a row of spherical droplets decreasing the total energy while conserving the volume. Plateau's theory was further promoted by the analytical work of Lord Rayleigh on the instability of liquid jets.¹⁸⁶ In the 1960's, Nichols and Mullins extended the concept to solid cylinders where mass transport is dominated by surface diffusion^a.¹⁸⁷ Experimental studies on the stability of gold and copper nanowires (diameters between 25 and 100 nm) revealed their fragmentation at elevated temperatures (400-600°C) and its dependency on annealing time, temperature, and wire diameter.^{188,189} Increasing the temperature accelerated diffusion and consequently, the fragmentation process. Thinner wires fragmented faster because atom diffusion is proportional to the gradient of the mean curvature of the wire surface.¹⁸⁷ The strong dependency on the wire diameter already hints that ultrathin gold nanowires with diameters below 2 nm will severely suffer from fragmentation by Rayleigh instability. In 2013, Xu et al. showed that AuNWs tend to transform into spheres even at room temperature.¹⁹⁰ They investigated the fragmentation of AuNWs inside block copolymer/AuNW hybrid cylindrical micelles and inside liquid dispersions by UV-vis spectroscopy and TEM analysis^b. AuNWs dispersed in THF transformed into spherical nanoparticles already after 18 h at room temperature; a temperature increase to 50°C accelerated the process to 5 min. Fragmentation by the energy input of an electron during electron microscopy analysis was also reported by several groups.^{168,176,191}

^a Cylinders with initial radius r and a sinusoidal perturbation $r = r_0 + \Delta r_0 \sin(2\pi x/\lambda)$ become unstable if the wavelength of the perturbation is larger than the rod circumference $2\pi r$.

^b They made use of the Rayleigh instability to create rows of spherical nanoparticles with defined diameter and spacing.

3 Results

3.1 Publication A: Sintering of Ultrathin Gold Nanowires for Transparent Electronics.

(DOI: [10.1021/acsami.5b02088](https://doi.org/10.1021/acsami.5b02088))

3.2 Publication B: Ultrathin Gold Nanowires for Transparent Electronics: Soft Sintering and Temperature Stability.

(DOI: [10.1002/pssa.201532874](https://doi.org/10.1002/pssa.201532874))

3.3 Publication C: Templated Self-Assembly of Ultrathin Gold Nanowires by Nanoimprinting for Transparent Flexible Electronics.

(DOI: [10.1021/acs.nanolett.5b04319](https://doi.org/10.1021/acs.nanolett.5b04319))

3.4 Publication D: Direct Nanoimprinting of a Colloidal Self-organizing Nanowire Ink for Transparent, Flexible Electronics.

(DOI: [10.1002/admt.201700034](https://doi.org/10.1002/admt.201700034))

4 Discussion

4.1 Sintering of AuNWs

AuNWs have unusual properties (small diameters, high aspect ratios, mechanical flexibility) that make them interesting as building blocks for TEs, but two limitations are commonly reported in literature: high electrical resistance and poor stability (see section 2.4.3). The same limitations were observed in this work: dip-coated layers of densely packed AuNWs on glass (see Figure 1 in publication A) exhibited sheet resistances larger than 40 M Ω ; after storage of 1 week at room temperature, pronounced fragmentation of the wires into spheres was observed (see Figure 4 in publication A). The most common approach to reduce contact resistances and improve conductivity in nanoparticle layers is a post-deposition sintering treatment that removes the organic ligand shell and induces coalescence of the nanoparticles (see section 2.3). Established thermal sintering techniques did not perform well with ultrathin wires: the Rayleigh instability (already present at room temperature) is significantly accelerated with increasing temperature (see section 2.4.3). The high boiling point of OAm (> 350°C) requires high sintering temperatures for ligand removal. Wires disintegrated into unconnected spheres before conductive pathways were obtained.¹⁹² Alternative sintering approaches that were reported in literature to effectively sinter nanoparticle inks without thermal impact include chemical (see section 2.3.2) and plasma sintering (see section 2.3.3). Both were examined for sintering AuNW layers in publication A.

For chemical sintering, the specific anchoring group of the ligand molecule to the particle surface plays a crucial role. AuNWs are capped by OAm, which binds with its amine moiety to the gold surface. Fafarman et al. reported a protocol to replace insulating OAm tethered to spherical gold nanoparticles by the short inorganic ammoniumthiocyanate (see section 2.3.2).¹²⁵ They observed a clear insulator-to-metal transition upon ligand exchange. AuNW layers treated by the same ligand exchange protocol increased conductivity, too, but the sheet resistance remained in the M Ω range (see publication A). SEM analysis revealed obvious changes in the layer morphology (see Figure 2 in

publication A). The wires apparently became mobile in the solution and agglomerated. Deterioration of the protecting OAm ligand shell during the dynamic ligand exchange process probably destabilized the wires leading to destruction of the film.

Plasma treatment in H₂/Ar atmosphere was shown to successfully sinter ultrathin wires and significantly improve the conductivity and stability of AuNW layers (see publication A). The process is operating at room temperature and is compatible to a variety of substrates like glass or polymer foils. Several papers adapted the procedure to turn AuNW films conductive.^{193,194} The following hypothesis explains the efficient sintering in the plasma atmosphere: In the reactive plasma atmosphere, OAm is decomposed and removed; the unprotected metal cores of the wires then fuse together by surface diffusion, probably assisted by soft sputtering processes (see section 2.3.3). Wires with ultrathin diameter have high surface to volume ratios and, thus, a high driving force to reduce free surface energy. Therefore, the unprotected wire surfaces already fuse without additional thermal impact that may cause fragmentation into spheres (see section 2.3). The hypothesis is supported by experimental results (see publication B): Raman spectroscopy indicated the thorough removal of oleylamine after sintering; characteristic peaks of OAm vanished below the detection limit (see Figure 3 in publication B). Electron microscopy proved the fusion of single wires into larger superstructures (see Figure 2 in publication A and Figure 2b in publication B); XRD measurements revealed an increase in crystallite size (see Figure 2c in publication B). Plasma sintering induced defects, too. Nanopores and grain boundaries (see Figure 2b in publication B) were responsible for the deviation from the bulk resistivity of gold.

The formation of larger superstructures is beneficial in two ways: (1) Enhanced electron transport: The sintered superstructures provide a larger wire cross sectional area reducing the contribution of electron surface scattering.^{56,184} (2) Increased stability: Rayleigh instability is less effective for larger structures (see section 2.4.3). Sintered layers in publication A were stable for at least 2 years. Interestingly, short plasma treatments of 1 min that largely retained the initial structure of the layer decreased the resistance, but accelerated the fragmentation process; already after few hours, a clear color change indicated a fragmentation into spheres (see Figure 4 in publication A). It is likely that OAm was only partially removed during the first minute without significant coalescence of the wires (see Figure 2 in publication A). Apparently, OAm is protecting the wires

and inhibiting Rayleigh instability. The hypothesis has been supported by a recent study of Takahata et al. who investigated the fragmentation of ultrathin gold nanorods (1.6 nm diameter, 20 nm length) in dispersion by time-resolved optical spectroscopy.¹⁹⁵ They point out the specific role of the OAm ligand shell on the surface diffusion of Au atoms and the associated influence on stability: high OAm densities impede the migration of Au atoms and can slow down the fragmentation process.^{195,196}

On the other hand, larger structures should also cause more optical scattering.⁷⁹ The haze was, however, consistently found to be less than $< 2\%$ for dip-coated layers (see publication B). Electron microscopy proved that sintering of the wires occurred locally at the nanoscale and the overall morphology of the layer remained virtually unchanged at the length scale that dominates optical scattering.

The optoelectronic performance of the dip-coated layers presented in publication A and B was limited by their morphology (homogeneous AuNW thin films with sparsely distributed unconnected nanowire bundles on top, see Figure 1b in publication A). Layers in publication A with an average thickness of ~ 10 nm had an average transmittance of only $T = 66\%$ at a sheet resistance of $R_s = 50 \Omega/\text{sq}$ after H_2/Ar -plasma sintering. Simply reducing the layer thickness did not improve the layer performance. Thinner layers with transmittances $T \geq 90\%$ showed poor electrical conductivity and stability. SEM analysis revealed partial decomposition of the thinner layers during plasma sintering (probably due to sputtering effects) and dewetting upon storage at room-temperature similar to thin evaporated metal layers.^{197–199} Elevated temperatures accelerated the dewetting process (see publication B).^a Interestingly, thicker wire bundles that were deposited on top remained stable and conductive (see Figure 5 in publication B).^b The results indicate a “critical wire density” necessary to effectively fuse the wires and create stable superstructures. This intrinsically limits the performance of homogeneous AuNW thin films: to achieve high transmittances the layers have to be very thin (i.e. mono or double layer¹⁷⁸), but structural decomposition will limit the electronic performance. Significant electron surface scattering further impedes the electron flow in ultrathin layers.

^a The described degradation processes should not be confused with the fragmentation by Rayleigh instability discussed for single wires. Both occur at different length scales.

^b Because the wire bundles were unconnected in the dip-coated layers, the overall electrical response of the dip-coated layers was mainly determined by the dense wire layers.

Patterning into grids could solve this problem (see also section 2.1.4): thicker wire bundles^a that are separated by voids could combine high stability and superior electrical transport with high optical transmittance.

4.2 Patterning of AuNWs

Printing ordered grids from nanoparticle inks has been largely restricted to spherical particles (see section 2.2).³⁰ Anisotropic particles could reduce the number of high-ohmic wire-wire contacts and improve conductivity, but stiff wires like AgNWs do not easily bend around the large curvatures of small grids. Their limited mobility will impede printing. AuNWs behave differently: their geometry lends them high mobility and mechanical flexibility (see Figure S1 in publication C).

The novel imprinting process introduced in publication C relies on the high mobility and flexibility of the wires. Dispersed wires follow the grid structure of a pre-patterned elastomeric stamp. During imprinting, the solvent evaporates through the stamp and the nanowires are deposited. The process resembles classical nanoimprinting, but differs in the way material is patterned: in classical nanoimprinting, the material is in full contact with the stamp immediately before peeling so that the stamp's features are precisely replicated; in the process developed in this work, an ink is patterned with a solid content far below 100%. A gold concentration of 4 mg/mL is equivalent to only 0.25 vol% of solid content, for example (see publication D). Hence, there is no direct contact between stamp and printed material after solvent evaporation, which eases the peeling of the stamp. The low solid content, however, entails also challenges: it has to be ensured that the wires form defined lines (high pattern fidelity) and are electrically connected over macroscopic areas (low sheet resistance). Key role for the successful printing plays the self-assembly^b of the wires into hierarchical bundles upon solvent evaporation: (1) Line contacts between the wires provoke well-defined bundles of parallel wires, which accumulate all metal. The size of the bundles and thus the linewidth can be tuned by the wire concentration in the ink. Linewidths down to 250 nm could be achieved with a pil-

^a Bundles provide critical wire density → sintered structures are stable against fragmentation and dewetting; enhanced electron transport due to larger wire cross sectional area.

^b In publication D, we used the term “self-organization” to stress the interplay between wire self-assembly and liquid motion.

lar spacing of 1 μm . (2) Percolation over macroscopic distances: The wires intercalate inside the bundles like wool fibers inside yarn and form an interconnected network over the whole grid at low gold concentration. Spherical particles at low concentrations tend to form unconnected clusters rather than a continuous network.

The plasma sintering protocol (15 min treatment in H_2/Ar plasma) was successfully applied to the printed grids, too. The self-assembly of the wires into bundles ensured locally a critical wire density and a successful sintering into conductive superstructures. Conductive meshes were obtained with properties ($T = 92\%$; $R_s = 227 \Omega/\text{sq}$) that fulfill the requirements for touch screen applications (see section 2.1.1). The grids had better bending stability than commercial ITO; their sheet resistance changed less than 6% after 450 bending cycles at a bending radius of 5 mm. The grids outperformed unpatterned, homogeneous layers with comparable transmittance regarding conductivity and stability. Printing defects that locally caused a reduced wire density and unconnected wire bundles (e.g. by insufficiently filled stamp cavities, impurities, stamp defects, etc.) led to dewetting at these spots after plasma sintering (see previous section). The overall resistance increased over time for such samples as percolating pathways got interrupted.

The process described in publication C (batch process; stamp in full contact with substrate) is limited regarding throughput and patterned area. Scale-up by simply using larger stamps did not result in homogeneous and successful printing. Significant swelling of the PDMS stamp by the organic solvents of the ink impeded conformal contact and homogeneous contact pressure. A thorough search for appropriate stamp materials that combine high solvent permeation and low swelling revealed that both properties are mutually dependent.²⁰⁰ The semi-continuous rolling configuration in publication D solved this issue in a different approach: in the rolling configuration, the effective ink-stamp contact area and time are decreased, which enables sufficient solvent evaporation throughout the stamp at limited swelling rate. The process was used to fabricate grids with different geometries (squares, lines, hexagons) on large areas up to 30 cm^2 . Grids were successfully printed on a variety of substrates (glass, PET foil, cling wrap, paper) with high pattern fidelity. The resulting layers showed optoelectronic properties comparable to ITO ($T > 92\%$, R_s down to 106 Ω/sq), but superior mechanical flexibility (see Figure 5 in publication D) and were applied in capacitive and resistive touch sensors (see Figure 6 in publication D). The larger linewidths obtained in publication D (0.9-

1.7 μm) compared to publication C (0.25-0.6 μm) are a result of the larger pillar spacing of the master (publication D: 1.8 μm , publication C: 1 μm) and different drying behavior caused by the process: in the rolling configuration, solvent uptake by the stamp is strongly influenced by the movement of the roller and the resulting flow characteristics of the ink inside the cavities (see sections 2.1 and 2.3 in publication D)

The combination of nanoimprinting and self-assembly makes “active” use of the colloidal properties of the nanoparticles. Particle interactions at the nanoscale control the formation of the final macroscopic structure. The self-assembly is key to achieve grids with superior resolution compared to established printing processes of nanoparticle inks, which usually have linewidths of several micrometer ($> 5\mu\text{m}$) and require large separation of the lines (\sim several hundreds of μm) in order to obtain high transmittance (see section 2.2 and Table 1, publication C). A pitch of 4 μm was sufficient to obtain $T = 92\%$ at a linewidth of 250 nm (publication C). Direct nanoimprinting of AuNWs is versatile, arbitrary structures can be printed by appropriate stamp design. The process does not require complex printing setup and allows for fast patterning; 30 cm^2 could be printed in 12 seconds (publication D). Larger stamps could further speed up the process. The complete process (patterning + sintering) is performed at room temperature, which reduces the thermal budget and makes it compatible with soft substrates like polymer foils or paper.

5 Conclusions

Ultrathin AuNWs have been introduced as promising base material with outstanding properties for the bottom-up fabrication of transparent electrodes, but also with many trade-offs. Table 1 summarizes the various characteristic properties of the wires and the corresponding effects on the performance as building blocks for transparent electronics.

Table 1: Properties of AuNWs for transparent electronics

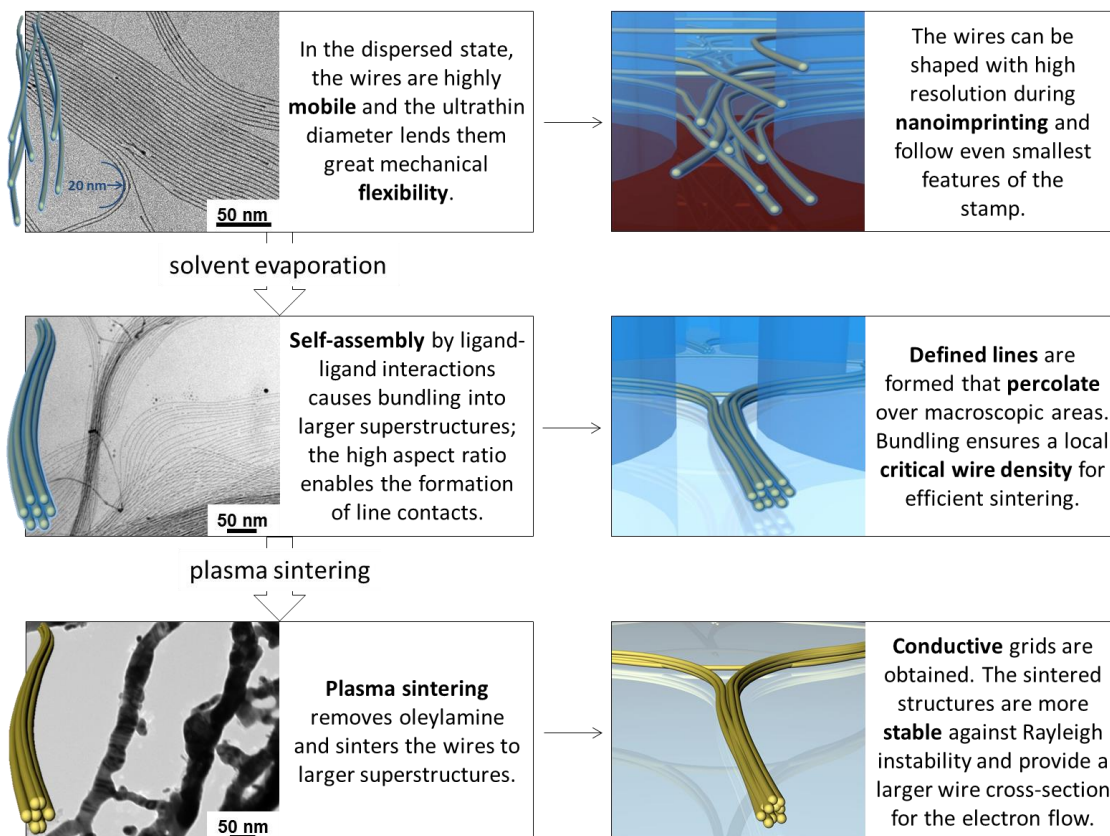
AuNWs for transparent electronics	
Opportunities	Challenges
small diameter	
+ flexibility + less scattering → high transmittance	– electron surface scattering → resistivity – fragmentation by Rayleigh instability – high surface to volume ratio → large organic fraction → contact resistance
high aspect ratio	
+ eases percolation + enables line contacts between wires → self-assembly	– needs to be bend to fit into features
OAm ligand shell	
+ enables self-assembly	– high contact resistances
material: gold	
+ chemical inertness + low diffusivity	– price ^a

In this thesis, a complete process was developed to apply AuNWs in TEs making use of the beneficial properties of AuNWs and addressing the limiting factors. Several post-deposition sintering treatments were investigated to reduce the large contact resistances and increase the stability of AuNW layers. H₂/Ar-plasma treatment was found to effi-

^a Metal costs usually play a smaller role in the total costs of production.

ciently remove the oleylamine ligand shell and fuse the wires into larger superstructure that resisted fragmentation by Rayleigh instability. The resistance of dip-coated AuNW layers decreased by 6 orders of magnitude after plasma treatment.

Patterning AuNW layers further enhanced the optoelectronic performance for TEs and increased layer stability. A novel nanoimprinting process was developed to pattern AuNWs into grids with superior resolution (linewidths down to 250 nm) to most of the state-of-the-art grids printed from nanoparticle inks. The developed process made use of the specific wire properties at the precise moment during the process enabling the fabrication of high-end metal grids for TEs:



The obtained grids showed **competitive optoelectronic properties to ITO** ($T > 92\%$ and R_s down to $106 \Omega/\text{sq}$), while fulfilling the requirements of novel polymer-based devices: **mechanical flexibility** and **low temperature processing**.

6 Outlook

Transparent electrode materials other than ITO are expected to represent a major part of the entire TE market in the next decade.²⁰¹ Although metal grids and metal nanowire networks were shown to reach competitive properties to ITO, their breakthrough will probably depend on how fast new applications like flexible devices that do not perform with ITO will enter the market.

This thesis proved the usability of AuNWs as nanoscale building block for the fabrication of transparent and flexible metal grids. Future work could include:

- Transfer the nanoimprinting process to continuous roll-to-roll processing. Accompanied with that, in-line sintering of the wires (for instance by atmospheric plasma) would have to be investigated.
- The combination of direct nanoimprinting and self-assembly of ultrathin wires is not restricted to gold. The pivotal properties for the process are not intrinsic properties of gold, but are determined by the geometry and the specific ligand interactions of the wires. Thus, exchange of the core material should not significantly affect the printing process and could open up new opportunities.
- The method could be extended to novel nanoparticle inks that are responsive to external stimuli like light, magnetic fields or temperature in order to specifically trigger the assembly during the imprinting process.
- Future hierarchical printing processes could combine local nanoscale patterns (to tune the material properties) with macroscopic circuit patterns in a single stamp. Patterned electrodes, as required for capacitive touch screen, for instance, could be fabricated in a single step. TEs like ITO or random AgNW layers have to be patterned after layer deposition in an additional process step.

7 Bibliography

- (1) Smartphone Usage Statistics 2014 - UK Survey of Smartphone Users | Tecmark <http://www.tecmark.co.uk/smartphone-usage-data-uk-2014/> (accessed Feb 7, 2017).
- (2) Hecht, D. S.; Hu, L.; Irvin, G. Emerging Transparent Electrodes Based on Thin Films of Carbon Nanotubes, Graphene, and Metallic Nanostructures. *Adv. Mater.* **2011**, *23*, 1482–1513.
- (3) Ellmer, K. Past Achievements and Future Challenges in the Development of Optically Transparent Electrodes. *Nat. Photonics* **2012**, *6*, 808–816.
- (4) Morag, A.; Jelinek, R. “Bottom-Up” Transparent Electrodes. *J. Colloid Interface Sci.* **2016**, *482*, 267–289.
- (5) Ye, S.; Rathmell, A. R.; Chen, Z.; Stewart, I. E.; Wiley, B. J. Metal Nanowire Networks: The Next Generation of Transparent Conductors. *Adv. Mater.* **2014**, *26*, 6670–6687.
- (6) Wright, A. W. On the Production of Transparent Metallic Film by the Electrical Discharge in Exhausted Tubes. *Am. J. Sci.* **1877**, *13*, 49–55.
- (7) Ghaffarzadeh, K.; Yamamoto, Y.; Zervos, H. *Conductive Ink Markets 2016-2026: Forecasts, Technologies, Players*; IDTechEx Ltd: Boston, MA, USA, 2016.
- (8) Progress in conductive ink-based transparent conductive films | Printed Electronics World <http://www.printedelectronicsworld.com/articles/10023/progress-in-conductive-ink-based-transparent-conductive-films?rsst2id=1> (accessed Jan 2, 2017).
- (9) *Organic Solar Cells*; Choy, W. C. H., Ed.; Green Energy and Technology; Springer London: London, 2013.
- (10) Brabec, C. J.; Sariciftci, N. S.; Hummelen, J. C. Plastic Solar Cells. *Adv. Funct. Mater.* **2001**, *11*, 15–26.
- (11) Frohne, H.; Shaheen, S. E.; Brabec, C. J.; Müller, D. C.; Sariciftci, N. S.; Meerholz, K. Influence of the Anodic Work Function on the Performance of Organic Solar Cells. *ChemPhysChem* **2002**, *3*, 795–799.
- (12) OLED Info | The OLED Experts <http://www.oled-info.com/> (accessed Jan 5, 2017).
- (13) Sannicolo, T.; Lagrange, M.; Cabos, A.; Celle, C.; Simonato, J.-P.; Bellet, D. Metallic Nanowire-Based Transparent Electrodes for Next Generation Flexible Devices: A Review. *Small* **2016**, *12*, 6052–6075.
- (14) Gordon, R. G. Criteria for Choosing Transparent Conductors. *MRS Bull.* **2000**, 52–57.
- (15) Hu, L.; Wu, H.; Cui, Y. Metal Nanogrids, Nanowires, and Nanofibers for Transparent Electrodes. *MRS Bull.* **2011**, *36*, 760–765.
- (16) Gaynor, W.; Hofmann, S.; Christoforo, M. G.; Sachse, C.; Mehra, S.; Salleo, A.; McGehee, M. D.; Gather, M. C.; Lüssem, B.; Müller-Meskamp, L.; *et al.* Color in the Corners: ITO-Free White OLEDs with Angular Color Stability. *Adv. Mater.* **2013**, *25*, 4006–4013.
- (17) Cravino, A.; Schilinsky, P.; Brabec, C. J. Characterization of Organic Solar Cells: The Importance of Device Layout. *Adv. Funct. Mater.* **2007**, *17*, 3906–3910.
- (18) Tvingstedt, K.; Inganäs, O. Electrode Grids for ITO-Free Organic Photovoltaic Devices. *Adv. Mater.* **2007**, *19*, 2893–2897.
- (19) Barnes, T. M.; Reese, M. O.; Bergeson, J. D.; Larsen, B. a.; Blackburn, J. L.; Beard, M. C.; Bult, J.; van de Lagemaat, J. Comparing the Fundamental Physics and Device Performance of

- Transparent, Conductive Nanostructured Networks with Conventional Transparent Conducting Oxides. *Adv. Energy Mater.* **2012**, *2*, 353–360.
- (20) Glover, R. E.; Tinkham, M. Conductivity of Superconducting Films for Photon Energies between 0.3 and 40kTc. *Phys. Rev.* **1957**, *108*, 243–256.
- (21) Dressel, M.; Grüner, G. *Electrodynamics of Solids: Optical Properties of Electrons in Matter*; Cambridge University Press, 2002.
- (22) Hu, L.; Hecht, D. S.; Grüner, G. Percolation in Transparent and Conducting Carbon Nanotube Networks. *Nano Lett.* **2004**, *4*, 2513–2517.
- (23) De, S.; King, P. J.; Lyons, P. E.; Khan, U.; Coleman, J. N. Size Effects and the Problem with Percolation in Nanostructured Transparent Conductors. *ACS Nano* **2010**, *4*, 7064–7072.
- (24) Kim, T.; Canlier, A.; Cho, C.; Rozyyev, V.; Lee, J.; Han, S. M. Highly Transparent Au-Coated Ag Nanowire Transparent Electrode with Reduction in Haze. *ACS Appl. Mater. Interfaces* **2014**, *6*, 13527–13534.
- (25) Chiba, Y.; Islam, A.; Komiya, R.; Koide, N.; Han, L. Conversion Efficiency of 10.8% by a Dye-Sensitized Solar Cell Using a TiO₂ Electrode with High Haze. *Appl. Phys. Lett.* **2006**, *88*, 223505.
- (26) Tang, Z.; Tress, W.; Inganäs, O. Light Trapping in Thin Film Organic Solar Cells. *Mater. Today* **2014**, *17*, 389–396.
- (27) Araki, T.; Jiu, J.; Nogi, M.; Koga, H.; Nagao, S.; Sugahara, T.; Suganuma, K. Low Haze Transparent Electrodes and Highly Conducting Air Dried Films with Ultra-Long Silver Nanowires Synthesized by One-Step Polyol Method. *Nano Res.* **2014**, *7*, 236–245.
- (28) Ok, K.-H.; Kim, J.; Park, S.-R.; Kim, Y.; Lee, C.-J.; Hong, S.-J.; Kwak, M.-G.; Kim, N.; Han, C. J.; Kim, J.-W. Ultra-Thin and Smooth Transparent Electrode for Flexible and Leakage-Free Organic Light-Emitting Diodes. *Sci. Rep.* **2015**, *5*, 9464.
- (29) Nam, S.; Song, M.; Kim, D.-H.; Cho, B.; Lee, H. M.; Kwon, J.-D.; Park, S.-G.; Nam, K.-S.; Jeong, Y.; Kwon, S.-H.; *et al.* Ultrasoother, Extremely Deformable and Shape Recoverable Ag Nanowire Embedded Transparent Electrode. *Sci. Rep.* **2014**, *4*, 4788.
- (30) Kamyshny, A.; Magdassi, S. Conductive Nanomaterials for Printed Electronics. *Small* **2014**, *10*, 3515–3535.
- (31) Drude, P. Zur Elektronentheorie Der Metalle. *Ann. Phys.* **1916**, *354*, 710–724.
- (32) Zhang, L.; Zhou, Y.; Guo, L.; Zhao, W.; Barnes, A.; Zhang, H.-T.; Eaton, C.; Zheng, Y.; Brahlek, M.; Haneef, H. F.; *et al.* Correlated Metals as Transparent Conductors. *Nat. Mater.* **2015**, *15*, 204–210.
- (33) Hummel, R. E. Atomistic Theory of the Optical Properties. In *Electronic Properties of Materials*; Springer New York: New York, NY, 2011; pp. 227–246.
- (34) Dixon, S. C.; Scanlon, D. O.; Carmalt, C. J.; Parkin, I. P. N-Type Doped Transparent Conducting Binary Oxides: An Overview. *J. Mater. Chem. C* **2016**, *419*, 462–465.
- (35) Zilberberg, K.; Riedl, T. Metal-Nanostructures – A Modern and Powerful Platform to Create Transparent Electrodes for Thin-Film Photovoltaics. *J. Mater. Chem. A* **2016**, *4*, 14481–14508.
- (36) Edwards, P. P.; Porch, A.; Jones, M. O.; Morgan, D. V.; Perks, R. M. Basic Materials Physics of Transparent Conducting Oxides. *Dalton Trans.* **2004**, 2995–3002.
- (37) Mizoguchi, H.; Kamiya, T.; Matsuishi, S.; Hosono, H. A Germanate Transparent Conductive Oxide. *Nat. Commun.* **2011**, *2*, 470.
- (38) Guo, C. F.; Ren, Z. Flexible Transparent Conductors Based on Metal Nanowire Networks. *Mater. Today* **2015**, *18*, 143–154.
- (39) Layani, M.; Kamyshny, A.; Magdassi, S. Transparent Conductors Composed of Nanomaterials. *Nanoscale* **2014**, *6*, 5581–5591.

- (40) Consolidation in transparent conductive film industry taking its toll | Printed Electronics World <http://www.printedelectronicsworld.com/articles/9078/consolidation-in-transparent-conductive-film-industry-taking-its-toll> (accessed Apr 28, 2017).
- (41) ITO alternatives: printed metal mesh is on the rise? | IDTechEx Research Article <http://www.idtechex.com/research/articles/ito-alternatives-printed-metal-mesh-is-on-the-rise-00010598.asp> (accessed May 9, 2017).
- (42) Hecht, D. S.; Kaner, R. B. Solution-Processed Transparent Electrodes. *MRS Bull.* **2011**, *36*, 749–755.
- (43) Heraeus. Conductive, Transparent and Flexible Polymers https://www.heraeus.com/en/group/products_and_solutions_group/conductive_polymers/conductive-polymers-home.aspx (accessed Jan 5, 2017).
- (44) Kim, Y. H.; Sachse, C.; MacHala, M. L.; May, C.; Müller-Meskamp, L.; Leo, K. Highly Conductive PEDOT:PSS Electrode with Optimized Solvent and Thermal Post-Treatment for ITO-Free Organic Solar Cells. *Adv. Funct. Mater.* **2011**, *21*, 1076–1081.
- (45) Huang, J.; Miller, P. F.; Wilson, J. S.; De Mello, A. J.; De Mello, J. C.; Bradley, D. D. C. Investigation of the Effects of Doping and Post-Deposition Treatments on the Conductivity, Morphology, and Work Function of poly(3,4- Ethylenedioxythiophene)/poly(styrene Sulfonate) Films. *Adv. Funct. Mater.* **2005**, *15*, 290–296.
- (46) Dimitriev, O. P.; Grinko, D. A.; Noskov, Y. V.; Ogurtsov, N. A.; Pud, A. A. PEDOT:PSS Films-Effect of Organic Solvent Additives and Annealing on the Film Conductivity. *Synth. Met.* **2009**, *159*, 2237–2239.
- (47) Tenent, R. C.; Barnes, T. M.; Bergeson, J. D.; Ferguson, A. J.; To, B.; Gedvilas, L. M.; Heben, M. J.; Blackburn, J. L. Ultrasoother, Large-Area, High-Uniformity, Conductive Transparent Single-Walled-Carbon-Nanotube Films for Photovoltaics Produced by Ultrasonic Spraying. *Adv. Mater.* **2009**, *21*, 3210–3216.
- (48) Dan, B.; Irvin, G. C.; Pasquali, M. Continuous and Scalable Fabrication of Transparent Conducting Carbon Nanotube Films. *ACS Nano* **2009**, *3*, 835–843.
- (49) Mirri, F.; Ma, A. W. K.; Hsu, T. T.; Behabtu, N.; Eichmann, S. L.; Young, C. C.; Tsentelovich, D. E.; Pasquali, M. High-Performance Carbon Nanotube Transparent Conductive Films by Scalable Dip Coating. *ACS Nano* **2012**, *6*, 9737–9744.
- (50) Geim, A. K.; Novoselov, K. S. The Rise of Graphene. *Nat. Mater.* **2007**, *6*, 183–191.
- (51) Wassei, J. K.; Kaner, R. B. Graphene, a Promising Transparent Conductor. *Mater. Today* **2010**, *13*, 52–59.
- (52) Bae, S.; Kim, H.; Lee, Y.; Xu, X.; Park, J.-S.; Zheng, Y.; Balakrishnan, J.; Lei, T.; Ri Kim, H.; Song, Y. Il; *et al.* Roll-to-Roll Production of 30-Inch Graphene Films for Transparent Electrodes. *Nat. Nanotechnol.* **2010**, *5*, 574–578.
- (53) Li, X. S.; Zhu, Y. W.; Cai, W. W.; Borysiak, M.; Han, B. Y.; Chen, D.; Piner, R. D.; Colombo, L.; Ruoff, R. S. Transfer of Large-Area Graphene Films for High-Performance Transparent Conductive Electrodes. *Nano Lett.* **2009**, *9*, 4359–4363.
- (54) Polat, E. O.; Balci, O.; Kakenov, N.; Uzlu, H. B.; Kocabas, C.; Dahiya, R. Synthesis of Large Area Graphene for High Performance in Flexible Optoelectronic Devices. *Sci. Rep.* **2015**, *5*, 16744.
- (55) Chen, Y.; Gong, X. L.; Gai, J. G. Progress and Challenges in Transfer of Large-Area Graphene Films. *Adv. Sci.* **2016**, *3*, 1–15.
- (56) Dingle, R. B. The Electrical Conductivity of Thin Wires. *Proc. R. Soc. London. Ser. A. Math. Phys. Sci.* **1950**, *201*, 545–560.
- (57) Langley, D. P.; Lagrange, M.; Giusti, G.; Jiménez, C.; Bréchet, Y.; Nguyen, N. D.; Bellet, D. Metallic Nanowire Networks: Effects of Thermal Annealing on Electrical Resistance. *Nanoscale* **2014**, *6*, 13535–13543.

- (58) Mutiso, R. M.; Sherrott, M. C.; Rathmell, A. R.; Wiley, B. J.; Winey, K. I. Integrating Simulations and Experiments to Predict Sheet Resistance and Optical Transmittance in Nanowire Films for Transparent Conductors. *ACS Nano* **2013**, *7*, 7654–7663.
- (59) Yu, Z.; Li, L.; Zhang, Q.; Hu, W.; Pei, Q. Silver Nanowire-Polymer Composite Electrodes for Efficient Polymer Solar Cells. *Adv. Mater.* **2011**, *23*, 4453–4457.
- (60) Scardaci, V.; Coull, R.; Lyons, P. E.; Rickard, D.; Coleman, J. N. Spray Deposition of Highly Transparent, Low-Resistance Networks of Silver Nanowires over Large Areas. *Small* **2011**, *7*, 2621–2628.
- (61) Hu, L.; Kim, H. S.; Lee, J.; Peumans, P.; Cui, Y. Scalable Coating and Properties of Transparent, Flexible, Silver Nanowire Electrodes. *ACS Nano* **2010**, *4*, 2955–2963.
- (62) Song, M.; You, D. S.; Lim, K.; Park, S.; Jung, S.; Kim, C. S.; Kim, D. H.; Kim, D. G.; Kim, J. K.; Park, J.; *et al.* Highly Efficient and Bendable Organic Solar Cells with Solution-Processed Silver Nanowire Electrodes. *Adv. Funct. Mater.* **2013**, *23*, 4177–4184.
- (63) De, S.; Higgins, T. M.; Lyons, P. E.; Doherty, E. M.; Nirmalraj, P. N.; Blau, W. J.; Boland, J. J.; Coleman, J. N. Silver Nanowire Networks as Flexible, Transparent, Conducting Films: Extremely High DC to Optical Conductivity Ratios. *ACS Nano* **2009**, *3*, 1767–1774.
- (64) Lee, P.; Lee, J.; Lee, H.; Yeo, J.; Hong, S.; Nam, K. H.; Lee, D.; Lee, S. S.; Ko, S. H. Highly Stretchable and Highly Conductive Metal Electrode by Very Long Metal Nanowire Percolation Network. *Adv. Mater.* **2012**, *24*, 3326–3332.
- (65) Ye, S.; Stewart, I. E.; Chen, Z.; Li, B.; Rathmell, A. R.; Wiley, B. J. How Copper Nanowires Grow and How to Control Their Properties. *Acc. Chem. Res.* **2016**, *49*, 442–451.
- (66) Rathmell, A. R.; Wiley, B. J. The Synthesis and Coating of Long, Thin Copper Nanowires to Make Flexible, Transparent Conducting Films on Plastic Substrates. *Adv. Mater.* **2011**, *23*, 4798–4803.
- (67) Rathmell, A. R.; Bergin, S. M.; Hua, Y.-L.; Li, Z.-Y.; Wiley, B. J. The Growth Mechanism of Copper Nanowires and Their Properties in Flexible, Transparent Conducting Films. *Adv. Mater.* **2010**, *22*, 3558–3563.
- (68) Chen, Z.; Ye, S.; Stewart, I. E.; Wiley, B. J. Copper Nanowire Networks with Transparent Oxide Shells That Prevent Oxidation without Reducing Transmittance. *ACS Nano* **2014**, *8*, 9673–9679.
- (69) Transparent Conductive Films (TCF) 2016-2026: Forecasts, Markets, Technologies: IDTechEx <http://www.idtechex.com/research/reports/transparent-conductive-films-tcf-2016-2026-forecasts-markets-technologies-000480.asp> (accessed Jan 23, 2017).
- (70) Preston, C.; Xu, Y.; Han, X.; Munday, J. N.; Hu, L. Optical Haze of Transparent and Conductive Silver Nanowire Films. *Nano Res.* **2013**, *6*, 461–468.
- (71) Lee, J.-Y.; Connor, S. T.; Cui, Y.; Peumans, P. Solution-Processed Metal Nanowire Mesh Transparent Electrodes. *Nano Lett.* **2008**, *8*, 689–692.
- (72) Kumar, A.; Kulkarni, G. U. Evaluating Conducting Network Based Transparent Electrodes from Geometrical Considerations. *J. Appl. Phys.* **2016**, *119*, 15102.
- (73) Neyts, K.; Real, A.; Marescaux, M.; Mladenovski, S.; Beeckman, J. Conductor Grid Optimization for Luminance Loss Reduction in Organic Light Emitting Diodes. *J. Appl. Phys.* **2008**, *103*, 93113.
- (74) Catrysse, P. B.; Fan, S. Nanopatterned Metallic Films for Use as Transparent Conductive Electrodes in Optoelectronic Devices. *Nano Lett.* **2010**, *10*, 2944–2949.
- (75) Kuang, P.; Park, J. M.; Leung, W.; Mahadevapuram, R. C.; Nalwa, K. S.; Kim, T. G.; Chaudhary, S.; Ho, K. M.; Constant, K. A New Architecture for Transparent Electrodes: Relieving the Trade-off between Electrical Conductivity and Optical Transmittance. *Adv. Mater.* **2011**, *23*, 2469–2473.
- (76) Jang, S.; Jung, W.-B.; Kim, C.; Won, P.; Lee, S.-G.; Cho, K. M.; Jin, M. liang; An, C. J.; Jeon, H.-J.; Ko, S. H.; *et al.* A Three-Dimensional Metal Grid Mesh as a Practical Alternative to ITO.

- Nanoscale* **2016**, *8*, 14257–14263.
- (77) Van De Groep, J.; Spinelli, P.; Polman, A. Transparent Conducting Silver Nanowire Networks. *Nano Lett.* **2012**, *12*, 3138–3144.
- (78) Liu, W.; Fang, Y.; Xu, Y. F.; Li, X.; Li, L. H. The Effect of Grid Shape on the Properties of Transparent Conductive Films Based on Flexographic Printing. *Sci. China Technol. Sci.* **2014**, *57*, 2536–2541.
- (79) Bergin, S. M.; Chen, Y.-H.; Rathmell, A. R.; Charbonneau, P.; Li, Z.-Y.; Wiley, B. J. The Effect of Nanowire Length and Diameter on the Properties of Transparent, Conducting Nanowire Films. *Nanoscale* **2012**, *4*, 1996.
- (80) Lee, S.-M.; Chae, J.-S.; Kim, D.-Y.; Choi, K. C. Plasmonic Nanomeshes as Large-Area, Low-Resistive Transparent Electrodes and Their Application to ITO-Free Organic Light-Emitting Diodes. *Org. Electron.* **2014**, *15*, 3354–3361.
- (81) Wu, W.; Tassi, N. G. A Broadband Plasmonic Enhanced Transparent Conductor. *Nanoscale* **2014**, *6*, 7811–7816.
- (82) Lim, J. W.; Lee, Y. T.; Pandey, R.; Yoo, T.-H.; Sang, B.-I.; Ju, B.-K.; Hwang, D. K.; Choi, W. K. Effect of Geometric Lattice Design on Optical/electrical Properties of Transparent Silver Grid for Organic Solar Cells. *Opt. Express* **2014**, *22*, 26891.
- (83) Zou, J.; Yip, H.-L.; Hau, S. K.; Jen, A. K.-Y. Metal Grid/conducting Polymer Hybrid Transparent Electrode for Inverted Polymer Solar Cells. *Appl. Phys. Lett.* **2010**, *96*, 203301.
- (84) Wünscher, S.; Abbel, R.; Perelaer, J.; Schubert, U. S. Progress of Alternative Sintering Approaches of Inkjet-Printed Metal Inks and Their Application for Manufacturing of Flexible Electronic Devices. *J. Mater. Chem. C* **2014**, *2*, 10232–10261.
- (85) Ahn, B. Y.; Lorang, D. J.; Lewis, J. A. Transparent Conductive Grids via Direct Writing of Silver Nanoparticle Inks. *Nanoscale* **2011**, *3*, 2700–2702.
- (86) Jang, Y.; Kim, J.; Byun, D. Invisible Metal-Grid Transparent Electrode Prepared by Electrohydrodynamic (EHD) Jet Printing. *J. Phys. D: Appl. Phys.* **2013**, *46*, 155103.
- (87) Park, J.; Hwang, J. Fabrication of a Flexible Ag-Grid Transparent Electrode Using Ac Based Electrohydrodynamic Jet Printing. *J. Phys. D: Appl. Phys.* **2014**, *47*, 405102.
- (88) Schneider, J.; Rohner, P.; Thureja, D.; Schmid, M.; Galliker, P.; Poulikakos, D. Electrohydrodynamic NanoDrip Printing of High Aspect Ratio Metal Grid Transparent Electrodes. *Adv. Funct. Mater.* **2015**, *26*, 833–840.
- (89) Hong, S.; Yeo, J.; Kim, G.; Kim, D.; Lee, H.; Kwon, J.; Lee, H.; Lee, P.; Ko, S. H. Nonvacuum, Maskless Fabrication of a Flexible Metal Grid Transparent Conductor by Low-Temperature Selective Laser Sintering of Nanoparticle Ink. *ACS Nano* **2013**, *7*, 5024–5031.
- (90) Lee, D.; Paeng, D.; Park, H. K.; Grigoropoulos, C. P. Vacuum-Free, Maskless Patterning of Ni Electrodes by Laser Reductive Sintering of NiO Nanoparticle Ink and Its Application to Transparent Conductors. *ACS Nano* **2014**, *8*, 9807–9814.
- (91) Layani, M.; Gruchko, M.; Milo, O.; Balberg, I.; Azulay, D.; Magdassi, S. Transparent Conductive Coatings by Printing Coffee Ring Arrays Obtained at Room Temperature. *ACS Nano* **2009**, *3*, 3537–3542.
- (92) Deegan, R. D.; Bakajin, O.; Dupont, T. F. Capillary Flow as the Cause of Ring Stains from Dried Liquid Drops. *Nature* **1997**, *389*, 827–829.
- (93) Zhang, Z.; Zhang, X.; Xin, Z.; Deng, M.; Wen, Y.; Song, Y. Controlled Inkjetting of a Conductive Pattern of Silver Nanoparticles Based on the Coffee-Ring Effect. *Adv. Mater.* **2013**, *25*, 6714–6718.
- (94) Zhang, Z.; Zhu, W. Controllable Fabrication of a Flexible Transparent Metallic Grid Conductor Based on the Coffee Ring Effect. *J. Mater. Chem. C* **2014**, *2*, 9587–9591.
- (95) Higashitani, K.; McNamee, C. E.; Nakayama, M. Formation of Large-Scale Flexible Transparent

- Conductive Films Using Evaporative Migration Characteristics of Au Nanoparticles. *Langmuir* **2011**, *27*, 2080–2083.
- (96) Layani, M.; Magdassi, S. Flexible Transparent Conductive Coatings by Combining Self-Assembly with Sintering of Silver Nanoparticles Performed at Room Temperature. *J. Mater. Chem.* **2011**, *21*, 15378.
- (97) Magdassi, S.; Grouchko, M.; Berezin, O.; Kamyshny, A. Triggering the Sintering of Silver Nanoparticles at Room Temperature. *ACS Nano* **2010**, *4*, 1943–1948.
- (98) Malaquin, L.; Kraus, T.; Schmid, H.; Delamarche, E.; Wolf, H. Controlled Particle Placement through Convective and Capillary Assembly. *Langmuir* **2007**, *23*, 11513–11521.
- (99) Kim, H. S.; Lee, C. H.; Sudeep, P. K.; Emrick, T.; Crosby, A. J. Nanoparticle Stripes, Grids, and Ribbons Produced by Flow Coating. *Adv. Mater.* **2010**, *22*, 4600–4604.
- (100) Park, J. H.; Lee, D. Y.; Seung, W.; Sun, Q.; Kim, S.-W.; Cho, J. H. Metallic Grid Electrode Fabricated via Flow Coating for High-Performance Flexible Piezoelectric Nanogenerators. *J. Phys. Chem. C* **2015**, *119*, 7802–7808.
- (101) Winzer, M.; Kleiber, M.; Dix, N.; Wiesendanger, R. Fabrication of Nano-Dot- and Nano-Ring-Arrays by Nanosphere Lithography. *Appl. Phys. A Mater. Sci. Process.* **1996**, *63*, 617–619.
- (102) Ho, Y. H.; Chen, K. Y.; Liu, S. W.; Chang, Y. T.; Huang, D. W.; Wei, P. K. Transparent and Conductive Metallic Electrodes Fabricated by Using Nanosphere Lithography. *Org. Electron.* **2011**, *12*, 961–965.
- (103) Kwon, N.; Kim, K.; Sung, S.; Yi, I.; Chung, I. Highly Conductive and Transparent Ag Honeycomb Mesh Fabricated Using a Monolayer of Polystyrene Spheres. *Nanotechnology* **2013**, *24*, 235205.
- (104) Kwon, N.; Kim, K.; Heo, J.; Yi, I.; Chung, I. Study on Ag Mesh/ Conductive Oxide Hybrid Transparent Electrode for Film Heaters. *Nanotechnology* **2014**, *25*, 265702.
- (105) Kang, M. G.; Kim, M. S.; Kim, J. S.; Guo, L. J. Organic Solar Cells Using Nanoimprinted Transparent Metal Electrodes. *Adv. Mater.* **2008**, *20*, 4408–4413.
- (106) Transparent Conductive Films (TCF) 2015-2025: Forecasts, Markets, Technologies | Acute Market Reports <http://www.acutemarketreports.com/report/transparent-conductive-films-tcf-2015-2025-forecasts-markets-technologies> (accessed Jan 24, 2017).
- (107) Schiff, H.; Kristensen, A. Nanoimprint Lithography. In *Springer Handbook of Nanotechnology*; Bhushan, B., Ed.; Springer Berlin Heidelberg, 2007; pp. 239–278.
- (108) Lan, H.; Ding, Y. Nanoimprint Lithography. In *Lithography*; Wang, M., Ed.; InTech, 2010; pp. 457–494.
- (109) Guo, L. J. Nanoimprint Lithography: Methods and Material Requirements. *Adv. Mater.* **2007**, *19*, 495–513.
- (110) Zhou, W. *Nanoimprint Lithography: An Enabling Process for Nanofabrication*; Springer Berlin Heidelberg, 2013.
- (111) Guo, L. J. Patterning Based on External Force: Nanoimprint Lithography. In *Unconventional Nanopatterning Techniques and Applications*; Rogers, J. A.; Lee, H. H., Eds.; John Wiley & Sons, Inc., 2008; pp. 129–166.
- (112) Ahn, S. H.; Guo, L. J. Large-Area Roll-to-Roll and Roll-to-Plate Nanoimprint Lithography: A Step toward High-Throughput Application of Continuous Nanoimprinting. *ACS Nano* **2009**, *3*, 2304–2310.
- (113) Ahn, S. H.; Guo, L. J. High-Speed Roll-to-Roll Nanoimprint Lithography on Flexible Plastic Substrates. *Adv. Mater.* **2008**, *20*, 2044–2049.
- (114) Stuart, C.; Chen, Y. Roll in and Roll out: A Path to High-Throughput Nanoimprint Lithography. *ACS Nano* **2009**, *3*, 2062–2064.

- (115) TEMICOAT - NANOIMPRINT TECHNOLOGIES <http://www.temicoat.com/> (accessed Jan 16, 2017).
- (116) Xia, Y.; Whitesides, G. M. Soft Lithography. *Annu. Rev. Mater. Sci.* **1998**, *28*, 153–184.
- (117) Qin, D.; Xia, Y.; Whitesides, G. M. Soft Lithography for Micro- and Nanoscale Patterning. *Nat. Protoc.* **2010**, *5*, 491–502.
- (118) Qin, D.; Xia, Y.; Whitesides, G. M. Soft Lithography for Micro- and Nanoscale Patterning. *Nat. Protoc.* **2010**, *5*, 491–502.
- (119) Cavallini, M.; Albonetti, C.; Biscarini, F. Nanopatterning Soluble Multifunctional Materials by Unconventional Wet Lithography. *Adv. Mater.* **2009**, *21*, 1043–1053.
- (120) Moonen, P. F.; Bat, E.; Voortthuijzen, W. P.; Huskens, J. Soft-Lithographic Patterning of Room Temperature-Sintering Ag Nanoparticles on Foil. *RSC Adv.* **2013**, *3*, 18498.
- (121) Duan, X.; Park, M.; Zhao, Y.; Berenschot, E.; Wang, Z.; Reinhoudt, D. N.; Rotello, V. M.; Huskens, J. Metal Nanoparticle Wires Formed by an Integrated Nanomolding-Chemical Assembly Process : Fabrication and Properties. *ACS Nano* **2010**, *4*, 7660–7666.
- (122) Kim, E.; Xia, Y.; Whitesides, G. M. Micromolding in Capillaries: Applications in Materials Science. *J. Am. Chem. Soc.* **1996**, *118*, 5722–5731.
- (123) Ko, S. H.; Park, I.; Pan, H.; Grigoropoulos, C. P.; Pisano, A. P.; Luscombe, C. K.; Fréchet, J. M. J. Direct Nanoimprinting of Metal Nanoparticles for Nanoscale Electronics Fabrication. *Nano Lett.* **2007**, *7*, 1869–1877.
- (124) Liang, C.-C.; Liao, M.-Y.; Chen, W.-Y.; Cheng, T.-C.; Chang, W.-H.; Lin, C.-H. Plasmonic Metallic Nanostructures by Direct Nanoimprinting of Gold Nanoparticles. *Opt. Express* **2011**, *19*, 4768–4776.
- (125) Fafarman, A. T.; Hong, S.-H.; Caglayan, H.; Ye, X.; Diroll, B. T.; Paik, T.; Engheta, N.; Murray, C. B.; Kagan, C. R. Chemically Tailored Dielectric-to-Metal Transition for the Design of Metamaterials from Nanoimprinted Colloidal Nanocrystals. *Nano Lett.* **2013**, *13*, 350–357.
- (126) Park, I.; Ko, S. H.; Pan, H.; Grigoropoulos, C. P.; Pisano, A. P.; Fréchet, J. M. J.; Lee, E.-S.; Jeong, J.-H. Nanoscale Patterning and Electronics on Flexible Substrate by Direct Nanoimprinting of Metallic Nanoparticles. *Adv. Mater.* **2008**, *20*, 489–496.
- (127) Hu, P.; Li, K.; Chen, W.; Peng, L.; Chu, D.; O’Neill, W. Fabrication of an Organic Field Effect Transistor Using Nano Imprinting of Ag Inks and Semiconducting Polymers. *J. Micromechanics Microengineering* **2010**, *20*, 129802.
- (128) Yu, X.; Pham, J. T.; Subramani, C.; Creran, B.; Yeh, Y.-C.; Du, K.; Patra, D.; Miranda, O. R.; Crosby, A. J.; Rotello, V. M. Direct Patterning of Engineered Ionic Gold Nanoparticles via Nanoimprint Lithography. *Adv. Mater.* **2012**, *24*, 6330–6334.
- (129) Kim, J. Y.; Kotov, N. A. Charge Transport Dilemma of Solution-Processed Nanomaterials. *Chem. Mater.* **2014**, *26*, 134–152.
- (130) Boles, M. A.; Engel, M.; Talapin, D. V. Self-Assembly of Colloidal Nanocrystals: From Intricate Structures to Functional Materials. *Chem. Rev.* **2016**, *116*, 11220–11289.
- (131) Reiser, B.; Gonzalez-Garcia, L.; Kanelidis, I.; Maurer, J. H. M.; Kraus, T. Gold Nanorods with Conjugated Polymer Ligands: Sintering-Free Conductive Inks for Printed Electronics. *Chem. Sci.* **2016**, *7*, 4190–4196.
- (132) Yang, C.; Wong, C. P.; Yuen, M. M. F. Printed Electrically Conductive Composites: Conductive Filler Designs and Surface Engineering. *J. Mater. Chem. C* **2013**, *1*, 4052.
- (133) Roduner, E. Size Matters: Why Nanomaterials Are Different. *Chem. Soc. Rev.* **2006**, *35*, 583.
- (134) Qi, W. H.; Wang, M. P. Size and Shape Dependent Melting Temperature of Metallic Nanoparticles. *Mater. Chem. Phys.* **2004**, *88*, 280–284.
- (135) Buffat, P.; Borel, J. P. Size Effect on the Melting Temperature of Gold Particles. *Phys. Rev. A*

- 1976, 13, 2287–2298.
- (136) Cherrington, M.; Claypole, T. C.; Deganello, D.; Mabbett, I.; Watson, T.; Worsley, D. Ultrafast near-Infrared Sintering of a Slot-Die Coated Nano-Silver Conducting Ink. *J. Mater. Chem.* **2011**, 21, 7562–7564.
- (137) NIR-Technologie, Lösungen, Anwendungen und Trockner - Adphos Gruppe <http://www.adphos.com/de/> (accessed Jan 12, 2017).
- (138) Schroder, K. A.; McCool, S. C.; Furlan, W. F. Broadcast Photonic Curing of Metallic Nanoparticle Films. *NSTI-Nanotech* **2006**, 3, 198–201.
- (139) Hwang, Y. T.; Chung, W.-H.; Jang, Y. R.; Kim, H.-S. Intensive Plasmonic Flash Light Sintering of Copper Nano-Inks Using a Band-Pass Light Filter for Highly Electrically Conductive Electrodes in Printed Electronics. *ACS Appl. Mater. Interfaces* **2016**, 8, 8591–8599.
- (140) Niittynen, J.; Sowade, E.; Kang, H.; Baumann, R. R.; Mäntysalo, M. Comparison of Laser and Intense Pulsed Light Sintering (IPL) for Inkjet-Printed Copper Nanoparticle Layers. *Sci. Rep.* **2015**, 5, 8832.
- (141) Garnett, E. C.; Cai, W.; Cha, J. J.; Mahmood, F.; Connor, S. T.; Greyson Christoforo, M.; Cui, Y.; McGehee, M. D.; Brongersma, M. L. Self-Limited Plasmonic Welding of Silver Nanowire Junctions. *Nat. Mater.* **2012**, 11, 241–249.
- (142) Jiu, J.; Nogi, M.; Sugahara, T.; Tokuno, T.; Araki, T.; Komoda, N.; Suganuma, K.; Uchida, H.; Shinozaki, K. Strongly Adhesive and Flexible Transparent Silver Nanowire Conductive Films Fabricated with a High-Intensity Pulsed Light Technique. *J. Mater. Chem.* **2012**, 22, 23561.
- (143) Park, S.-H.; Jang, S.; Lee, D.-J.; Oh, J.; Kim, H.-S. Two-Step Flash Light Sintering Process for Crack-Free Inkjet-Printed Ag Films. *J. Micromechanics Microengineering* **2013**, 23, 15013.
- (144) Lee, D. J.; Park, S. H.; Jang, S.; Kim, H. S.; Oh, J. H.; Song, Y. W. Pulsed Light Sintering Characteristics of Inkjet-Printed Nanosilver Films on a Polymer Substrate. *J. Micromechanics Microengineering* **2011**, 21, 125023.
- (145) Printed Electronics Product Leadership | NovaCentrix <http://www.novacentrix.com/products/overview> (accessed Jan 12, 2017).
- (146) Gepulste Blitzlampen - Xenon und Krypton https://www.heraeus.com/de/hng/products_and_solutions/arc_and_flash_lamps/flash_lamps.aspx (accessed Jan 12, 2017).
- (147) Schroder, K. a; Suite, P. D. Mechanisms of Photonic CuringTM: Processing High Temperature Films on Low Temperature Substrates. *Nanotech Conf. Tech. Proc.* **2011**, 220–223.
- (148) Pilot Scale Roll to Roll | NovaCentrix <http://www.novacentrix.com/products/pulseforge/R2R> (accessed Jan 12, 2017).
- (149) Yung, K. C.; Gu, X.; Lee, C. P.; Choy, H. S. Ink-Jet Printing and Camera Flash Sintering of Silver Tracks on Different Substrates. *J. Mater. Process. Technol.* **2010**, 210, 2268–2272.
- (150) Ko, S. H.; Pan, H.; Grigoropoulos, C. P.; Luscombe, C. K.; Fréchet, J. M. J.; Poulidakos, D. All-Inkjet-Printed Flexible Electronics Fabrication on a Polymer Substrate by Low-Temperature High-Resolution Selective Laser Sintering of Metal Nanoparticles. *Nanotechnology* **2007**, 18, 345202.
- (151) Grouchko, M.; Kamyshny, A.; Mihailescu, C. F.; Anghel, D. F.; Magdassi, S. Conductive Inks with A “built-In” mechanism That Enables Sintering at Room Temperature. *ACS Nano* **2011**, 5, 3354–3359.
- (152) Fafarman, A. T.; Koh, W.; Diroll, B. T.; Kim, D. K.; Ko, D.-K.; Oh, S. J.; Ye, X.; Doan-Nguyen, V.; Crump, M. R.; Reifsnnyder, D. C.; *et al.* Thiocyanate-Capped Nanocrystal Colloids: Vibrational Reporter of Surface Chemistry and Solution-Based Route to Enhanced Coupling in Nanocrystal Solids. *J. Am. Chem. Soc.* **2011**, 133, 15753–15761.
- (153) Korner, N.; Beck, E.; Dommann, A.; Onda, N.; Ramm, J. Hydrogen Plasma Chemical Cleaning of Metallic Substrates and Silicon Wafers. *Surf. Coatings Technol.* **1995**, 76–77, 731–737.

- (154) Gehl, B.; Frömsdorf, A.; Aleksandrovic, V.; Schmidt, T.; Pretorius, A.; Flege, J.-I.; Bernstorff, S.; Rosenauer, A.; Falta, J.; Weller, H.; *et al.* Structural and Chemical Effects of Plasma Treatment on Close-Packed Colloidal Nanoparticle Layers. *Adv. Funct. Mater.* **2008**, *18*, 2398–2410.
- (155) Reinhold, I.; Hendriks, C. E.; Eckardt, R.; Kranenburg, J. M.; Perelaer, J.; Baumann, R. R.; Schubert, U. S. Argon Plasma Sintering of Inkjet Printed Silver Tracks on Polymer Substrates. *J. Mater. Chem.* **2009**, *19*, 3384–3388.
- (156) Cademartiri, L.; Ghadimi, A.; Ozin, G. A. Nanocrystal Plasma Polymerization : From Colloidal Nanocrystals to Inorganic Architectures. *Acc. Chem. Res.* **2008**, *41*, 1820–1830.
- (157) Wünsch, S.; Stumpf, S.; Teichler, A.; Pabst, O.; Perelaer, J.; Beckert, E.; Schubert, U. S. Localized Atmospheric Plasma Sintering of Inkjet Printed Silver Nanoparticles. *J. Mater. Chem.* **2012**, *22*, 24569–24576.
- (158) Zhang, A.; Zheng, G.; Lieber, C. *Nanowires : Building Blocks for Nanoscience and Nanotechnology*; Springer International Publishing, 2016.
- (159) Pei, L.; Mori, K.; Adachi, M. Formation Process of Two-Dimensional Networked Gold Nanowires by Citrate Reduction of AuCl₄⁻ and the Shape Stabilization. *Langmuir* **2004**, *20*, 7837–7843.
- (160) Kim, F.; Sohn, K.; Wu, J.; Huang, J. Chemical Synthesis of Gold Nanowires in Acidic Solutions. *J. Am. Chem. Soc.* **2008**, *130*, 14442–14443.
- (161) Liu, X.; Wu, N.; Wunsch, B. H.; Barsotti, R. J.; Stellacci, F. Shape-Controlled Growth of Micrometer-Sized Gold Crystals by a Slow Reduction Method. *Small* **2006**, *2*, 1046–1050.
- (162) Bai, H.; Xu, K.; Xu, Y.; Matsui, H. Fabrication of Au Nanowires of Uniform Length and Diameter Using a Monodisperse and Rigid Biomolecular Template: Collagen-like Triple Helix. *Angew. Chemie - Int. Ed.* **2007**, *46*, 3319–3322.
- (163) Forrer, P.; Schlotig, F.; Siegenthaler, H.; Textor, M. Electrochemical Preparation and Surface Properties of Gold Nanowire Arrays Formed by the Template Technique. *J. Appl. Electrochem.* **2000**, *30*, 533–541.
- (164) Cross, C. E.; Hemminger, J. C.; Penner, R. M. Physical Vapor Deposition of One-Dimensional Nanoparticle Arrays on Graphite: Seeding the Electrodeposition of Gold Nanowires. *Langmuir* **2007**, *23*, 10372–10379.
- (165) Halder, A.; Ravishankar, N. Ultrafine Single-Crystalline Gold Nanowire Arrays by Oriented Attachment. *Adv. Mater.* **2007**, *19*, 1854–1858.
- (166) Wang, C.; Hu, Y.; Lieber, C. M.; Sun, S. Ultrathin Au Nanowires and Their Transport Properties. *J. Am. Chem. Soc.* **2008**, *130*, 8902–8903.
- (167) Huo, Z.; Tsung, C.-K.; Huang, W.; Zhang, X.; Yang, P. Sub-Two Nanometer Single Crystal Au Nanowires. *Nano Lett.* **2008**, *8*, 2041–2044.
- (168) Pazos-Pérez, N.; Baranov, D.; Irsen, S.; Hilgendorff, M.; Liz-Marzán, L. M.; Giersig, M. Synthesis of Flexible, Ultrathin Gold Nanowires in Organic Media. *Langmuir* **2008**, *24*, 9855–9860.
- (169) Lu, X.; Yavuz, M. S.; Tuan, H.; Korgel, B. A.; Xia, Y. Ultrathin Gold Nanowires Can Be Obtained by Reducing Polymeric Strands of Oleylamine - AuCl Complexes Formed via Auophilic Interaction. *J. Am. Chem. Soc.* **2008**, *130*, 8900–8901.
- (170) Feng, H.; Yang, Y.; You, Y.; Li, G.; Guo, J.; Yu, T.; Shen, Z.; Wu, T.; Xing, B. Simple and Rapid Synthesis of Ultrathin Gold Nanowires, Their Self-Assembly and Application in Surface-Enhanced Raman Scattering. *Chem. Commun.* **2009**, 1984–1986.
- (171) Pong, B. K.; Lee, J. Y.; Trout, B. L. First Principles Computational Study for Understanding the Interactions between ssDNA and Gold Nanoparticles: Adsorption of Methylamine on Gold Nanoparticulate Surfaces. *Langmuir* **2005**, *21*, 11599–11603.
- (172) You, H.; Liu, X.; Liu, H.; Fang, J. Theoretical Description of the Role of Amine Surfactant on the Anisotropic Growth of Gold Nanocrystals. *CrystEngComm* **2016**, *18*, 3934–3941.

- (173) You, H.; Wang, W.; Yang, S. A Universal Rule for Organic Ligand Exchange. *ACS Appl. Mater. Interfaces* **2014**, *6*, 19035–19040.
- (174) Wang, C.; Hou, Y.; Kim, J.; Sun, S. A General Strategy for Synthesizing FePt Nanowires and Nanorods. *Angew. Chemie - Int. Ed.* **2007**, *46*, 6333–6335.
- (175) Loubat, A.; Impéror-Clerc, M.; Pansu, B.; Meneau, F.; Raquet, B.; Viau, G.; Lacroix, L.-M. Growth and Self-Assembly of Ultrathin Au Nanowires into Expanded Hexagonal Superlattice Studied by in Situ SAXS. *Langmuir* **2014**, *30*, 4005–4012.
- (176) Yu, Y.; Cui, F.; Sun, J.; Yang, P. Atomic Structure of Ultrathin Gold Nanowires. *Nano Lett.* **2016**, *16*, 3078–3084.
- (177) Sánchez-Iglesias, A.; Rivas-Murias, B.; Grzelczak, M.; Pérez-Juste, J.; Liz-Marzán, L. M.; Rivadulla, F.; Correa-Duarte, M. A. Highly Transparent and Conductive Films of Densely Aligned Ultrathin Au Nanowire Monolayers. *Nano Lett.* **2012**, *12*, 6066–6070.
- (178) Chen, Y.; Ouyang, Z.; Gu, M.; Cheng, W. Mechanically Strong, Optically Transparent, Giant Metal Superlattice Nanomembranes from Ultrathin Gold Nanowires. *Adv. Mater.* **2013**, *25*, 80–85.
- (179) Reiser, B.; Gerstner, D.; Gonzalez-Garcia, L.; Maurer, J. H. M.; Kanelidis, I.; Kraus, T. Multivalent Bonds in Self-Assembled Bundles of Ultrathin Gold Nanowires. *Phys. Chem. Chem. Phys.* **2016**, *18*, 27165–27169.
- (180) Gong, S.; Schwalb, W.; Wang, Y.; Chen, Y.; Tang, Y.; Si, J.; Shirinzadeh, B.; Cheng, W. A Wearable and Highly Sensitive Pressure Sensor with Ultrathin Gold Nanowires. *Nat. Commun.* **2014**, *5*, 1–8.
- (181) Gong, S.; Lai, D. T. H.; Su, B.; Si, K. J.; Ma, Z.; Yap, L. W.; Guo, P.; Cheng, W. Highly Stretchy Black Gold E-Skin Nanopatches as Highly Sensitive Wearable Biomedical Sensors. *Adv. Electron. Mater.* **2015**, *1*, 1400063.
- (182) Gong, S.; Lai, D. T. H.; Wang, Y.; Yap, L. W.; Si, K. J.; Shi, Q.; Jason, N. N.; Sridhar, T.; Uddin, H.; Cheng, W. Tattolike Polyaniline Microparticle-Doped Gold Nanowire Patches as Highly Durable Wearable Sensors. *ACS Appl. Mater. Interfaces* **2015**, *7*, 19700–19708.
- (183) Pud, S.; Kisner, A.; Heggen, M.; Belaineh, D.; Temirov, R.; Simon, U.; Offenhäusser, A.; Mourzina, Y.; Vitusevich, S. Features of Transport in Ultrathin Gold Nanowire Structures. *Small* **2013**, *9*, 846–852.
- (184) Sondheimer, E. H. The Mean Free Path of Electrons in Metals. *Adv. Phys.* **1952**, *1*, 1–42.
- (185) Plateau, J. . *Transl. Annu. Reports Smithson. Inst.* **1873**, 1863.
- (186) Rayleigh, Lord. On the Stability of Jets. *Proc. London Math. Soc.* **1878**, *10*, 4–12.
- (187) Nichols, F.A.; Mullins, W. W. Surface- (Interface-) and Volume-Diffusion Contribution to Morphological Changes Driven by Capillarity. *Trans. Met. Soc. AIME* **1965**, *233*, 1840–1848.
- (188) Karim, S.; Toimil-Molares, M. E.; Balogh, A. G.; Ensinger, W.; Cornelius, T. W.; Khan, E. U.; Neumann, R. Morphological Evolution of Au Nanowires Controlled by Rayleigh Instability. *Nanotechnology* **2006**, *17*, 5954–5959.
- (189) Toimil Molares, M. E.; Balogh, A. G.; Cornelius, T. W.; Neumann, R.; Trautmann, C. Fragmentation of Nanowires Driven by Rayleigh Instability. *Appl. Phys. Lett.* **2004**, *85*, 5337–5339.
- (190) Xu, J.; Zhu, Y.; Zhu, J.; Jiang, W. Ultralong Gold Nanoparticle/block Copolymer Hybrid Cylindrical Micelles: A Strategy Combining Surface Templated Self-Assembly and Rayleigh Instability. *Nanoscale* **2013**, *5*, 6344–6349.
- (191) Lacroix, L. M.; Arenal, R.; Viau, G. Dynamic HAADF-STEM Observation of a Single-Atom Chain as the Transient State of Gold Ultrathin Nanowire Breakdown. *J. Am. Chem. Soc.* **2014**, *136*, 13075–13077.
- (192) Gonzalez-Garcia, L.; Maurer, J. H. M.; Reiser, B.; Kanelidis, I.; Kraus, T. Ultrathin Gold

- Nanowires for Transparent Electronics: Breaking Barriers. *Procedia Eng.* **2016**, *141*, 152–156.
- (193) Gong, S.; Zhao, Y.; Yap, L. W.; Shi, Q.; Wang, Y.; Bay, J. A. P. B.; Lai, D. T. H.; Uddin, H.; Cheng, W. Fabrication of Highly Transparent and Flexible NanoMesh Electrode via Self-Assembly of Ultrathin Gold Nanowires. *Adv. Electron. Mater.* **2016**, 1600121.
- (194) He, Y.; Chen, Y.; Xu, Q.; Xu, J.; Weng, J. Assembly of Ultrathin Gold Nanowires into Honeycomb Macroporous Pattern Films with High Transparency and Conductivity. *ACS Appl. Mater. Interfaces* **2017**, *9*, 7826–7833.
- (195) Takahata, R.; Yamazoe, S.; Warakulwit, C.; Limtrakul, J.; Tsukuda, T. Rayleigh Instability and Surfactant-Mediated Stabilization of Ultrathin Gold Nanorods. *J. Phys. Chem. C* **2016**, *120*, 17006–17010.
- (196) Huber, S. E.; Warakulwit, C.; Limtrakul, J.; Tsukuda, T.; Probst, M. Thermal Stabilization of Thin Gold Nanowires by Surfactant-Coating: A Molecular Dynamics Study. *Nanoscale* **2012**, *4*, 585–590.
- (197) Thompson, C. V. Solid-State Dewetting of Thin Films. *Annu. Rev. Mater. Res.* **2012**, *42*, 399–434.
- (198) Hernadez-Cruz, O.; Avila-Gutierrez, L.; Zolotukhin, M. G.; Gonzalez, G.; Monroy, B. M.; Montiel, R.; Vera-Graziano, R.; Romero-Ibarra, J. E.; Novelo-Peralta, O.; Massoojas, F. A. Spontaneous, Solvent-Free, Polymer-Templated, Solid–Solid Transformation of Thin Metal Films into Nanoparticles. *Nano Lett.* **2016**, *16*, 5420–5425.
- (199) Müller, C. M.; Spolenak, R. Microstructure Evolution during Dewetting in Thin Au Films. *Acta Mater.* **2010**, *58*, 6035–6045.
- (200) Backes, I. K. Large-Area Nanoimprint of Ultrathin Gold Nanowires: Ink-Stamp Interplay, Saarland University and INM - Leibniz Institute for New Materials, 2016.
- (201) Transparent Conductive Films (TCF) 2017-2027: Forecasts, Markets, Technologies: IDTechEx <http://www.idtechex.com/research/reports/transparent-conductive-films-tcf-2017-2027-forecasts-markets-technologies-000524.asp> (accessed May 10, 2017).
- (202) Saw, K. G.; Aznan, N. M.; Yam, F. K.; Ng, S. S.; Pung, S. Y. New Insights on the Burstein-Moss Shift and Band Gap Narrowing in Indium-Doped Zinc Oxide Thin Films. *PLoS One* **2015**, *10*, 1–17.
- (203) Hamberg, I.; Granqvist, C. G.; Berggren, K. F.; Sernelius, B. E.; Engström, L. Band-Gap Widening in Heavily Sn-Doped In₂O₃. *Phys. Rev. B* **1984**, *30*, 3240–3249.

8 Appendix

8.1 List of abbreviations and symbols

AFM	Atomic force microscope
AgNP(s)	Silver nanoparticle(s)
AuNP(s)	Gold nanoparticle(s)
AgNW(s)	Silver nanowire(s)
AuNW(s)	Gold nanowire(s)
CuNW(s)	Copper nanowire(s)
GISAXS	Gracing-incidence small-angle X-ray scattering
<i>h</i>	Planck's constant
ITO	Indium tin oxide
LED	Light-emitting diode
NIR	Near-infrared
NM	Nanomesh
NP(s)	Nanoparticle(s)
OAm	Oleylamine
OLED(s)	Organic light-emitting diode(s)
OSC(s)	Organic solar cell(s)
PDMS	Polydimethylsiloxane
PEDOT:PSS	Poly(3,4-ethylenedioxythiophene):poly(styrenesulfonate)
PET	Polyethylene terephthalate
PTEBS	Poly[2-(3-thienyl)-ethyloxy-4-butylsulfonate]

ρ	Resistivity ($\Omega\cdot\text{m}$)
R2R	Roll-to-roll
R_s, R_{\square}	Sheet resistance (Ω/sq)
RF	Radio frequency
σ	Conductivity (S/m)
SAXS	Small-angle X-ray scattering
SEM	Scanning electron microscopy
T_{bal}	Ballistic optical transmittance (%)
T_{dif}	Diffuse optical transmittance (%)
T_{tot}	Total optical transmittance (%)
TE(s)	Transparent electrode(s)
TCM(s)	Transparent conductive material(s)
TCO(s)	Transparent conductive oxide(s)
TEM	Transmission electron microscope
UV	Ultraviolet
UV-vis	Ultraviolet-visible
XRD	X-ray diffraction

8.2 Sheet resistance

The electrical sheet resistance has been introduced as a measure of resistance for thin films with homogeneous thickness. For a three-dimensional conductor, the resistance of a material is determined by the resistivity ρ (in $\Omega \cdot \text{m}$, intrinsic material property) and the geometry (cross-sectional area $A = w \cdot t$, length l between contacts):

$$R = \rho \cdot \frac{l}{A} = \rho \cdot \frac{l}{w \cdot t}$$

For thin films, the resistivity divided by the thickness is defined as “sheet resistance” R_s , which is independent of the measured area:

$$R_s = \frac{\rho}{t}$$

The unit of the sheet resistance is ohm, but usually given as “ohm per square” (Ω/sq , Ω/\square) to distinguish from the resistance.

The resistance of a thin film is then related to the sheet resistance by:

$$R = \frac{\rho}{t} \cdot \frac{l}{w} = R_s \cdot \frac{l}{w}$$

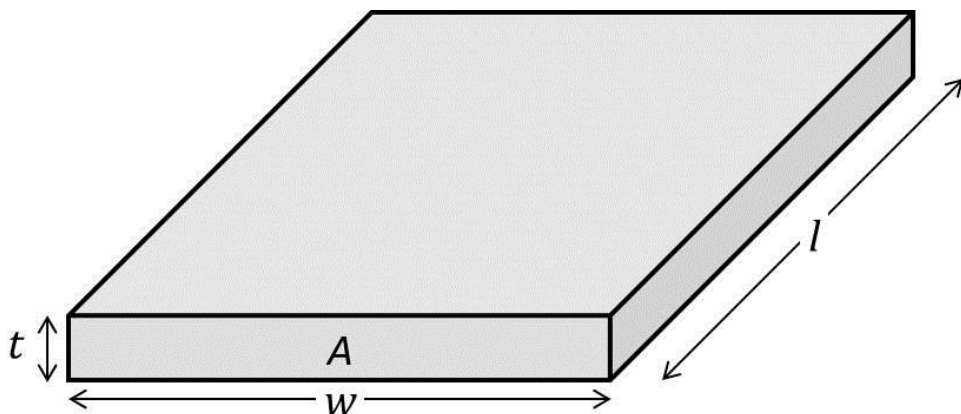


Figure 4: General geometry of a resistor with relevant parameters that affect the resistance.

8.3 List of publications

- (9) **Spinning Hierarchical Gold Nanowire Microfibers by Shear Alignment and Intermolecular Self-Assembly**
B. Reiser, D. Gerstner, L. González-García, **J. H. M. Maurer**, I. Kanelidis, and T. Kraus
ACS Nano, **2017**, 11, 4934-4942
- (8) **Direct nanoimprinting of a colloidal self-organizing nanowire ink for flexible, transparent electronics**
J. H. M. Maurer, L. González-García, I. K. Backes, B. Reiser, S. M. Schlossberg, and T. Kraus
Adv. Mater. Technol., **2017**, 1700034
- (7) **Multivalent bonds in self-assembled bundles of ultrathin gold nanowires**
B. Reiser, D. Gerstner, L. Gonzalez-Garcia, **J. H. M. Maurer**, I. Kanelidis, and T. Kraus
Phys. Chem. Chem. Phys., **2016**, 18, 27165-27169
- (6) **Ultrathin gold nanowires for transparent electronics: Soft sintering and temperature stability**
J. H. M. Maurer, L. González-García, B. Reiser, I. Kanelidis, and T. Kraus
Phys. Status Solidi A, **2016**, 213, 2336–2340
- (5) **Templated Self-Assembly of Ultrathin Gold Nanowires by Nanoimprinting for Transparent Flexible Electronics**
J. H. M. Maurer, L. González-García, B. Reiser, I. Kanelidis, and T. Kraus
Nano Lett., **2016**, 16, 2921-2925
- (4) **Gold nanorods with conjugated polymer ligands: sintering-free conductive inks for printed electronics**
B. Reiser, L. Gonzalez-Garcia, I. Kanelidis, **J. H.M. Maurer**, and T. Kraus
RSC Chem. Sci., **2016**, 7, 4190-4196
- (3) **Ultrathin gold nanowires for transparent electronics: breaking barriers**
L. González-García, **J. H. M. Maurer**, B. Reiser, I. Kanelidis and T. Kraus
Procedia Eng. **2016**, 141, 152–156
- (2) **Sintering of ultrathin gold nanowires for transparent electronics**
J. H. M. Maurer, L. González-García, B. Reiser, I. Kanelidis and T. Kraus
ACS Appl. Mater. Inter., **2015**, 7, 7838-7842
- (1) **Genetically improved monolayer-forming tobacco mosaic viruses to generate nanostructured semiconducting bio/inorganic hybrids**
P. Atanasova, N. Stitz, S. Sanctis, **J. H. M. Maurer**, R. C. Hoffmann, S. Eiben, H. Jeske, J. J. Schneider and J. Bill
Langmuir, **2015**, 31, 3897-3903

8.4 Conference contributions

Oral contributions:

LOPEC 2016, Munich, Germany

Oral presentation: “Direct nanoimprint of metal nanowires for transparent electronics”
Apr 5-7, 2016

EMRS Fall Meeting 2015, Warsaw, Poland

Oral presentation: “Soft Sintering of Ultrathin Gold Nanowires for Transparent Electronics”
Sep 15-18, 2015, **Materials Horizon best presentation award**

57th Electronic Materials Conference, Ohio State University, Columbus, OH, USA

Oral presentation: “Ultrathin gold nanowires for transparent electronics: decreasing the wire-wire junction resistance by annealing”
June 24-26, 2015

Poster contributions:

PhD Day 2016, Saarland University, Saarbrücken, Germany

Poster presentation: “Innovative ink concepts for transparent and printed electronics”
November 9, 2016

PhD Day 2014, Saarland University, Saarbrücken, Germany

Poster presentation: “Metal-Polymer Nanocomposites with structural control”
November 12, 2014

40th International Micro and Nano Engineering Conference (MNE), Swiss Tech Convention Center, Lausanne, Switzerland

Poster presentation: “Aligned metal nanostructures by convective self-assembly using pre-patterned transparent polymer”
September 22-26, 2014

